

## Subsurface volatile content of martian double-layer ejecta (DLE) craters



Donna Viola<sup>a,\*</sup>, Alfred S. McEwen<sup>a</sup>, Colin M. Dundas<sup>b</sup>, Shane Byrne<sup>a</sup>

<sup>a</sup>Lunar and Planetary Laboratory, University of Arizona, Tucson, AZ, 85721, USA

<sup>b</sup>Astrogeology Science Center, U.S. Geological Survey, Flagstaff, AZ, 86001, USA

### ARTICLE INFO

#### Article history:

Received 16 July 2016

Revised 16 November 2016

Accepted 21 November 2016

Available online 27 November 2016

#### Keywords:

Cratering

Ices

Impact processes

Mars, surface

### ABSTRACT

Excess ice is widespread throughout the martian mid-latitudes, particularly in Arcadia Planitia, where double-layer ejecta (DLE) craters also tend to be abundant. In this region, we observe the presence of thermokarstically-expanded secondary craters that likely form from impacts that destabilize a subsurface layer of excess ice, which subsequently sublimates. The presence of these expanded craters shows that excess ice is still preserved within the adjacent terrain. Here, we focus on a 15-km DLE crater that contains abundant superposed expanded craters in order to study the distribution of subsurface volatiles both at the time when the secondary craters formed and, by extension, remaining today. To do this, we measure the size distribution of the superposed expanded craters and use topographic data to calculate crater volumes as a proxy for the volumes of ice lost to sublimation during the expansion process. The inner ejecta layer contains craters that appear to have undergone more expansion, suggesting that excess ice was most abundant in that region. However, both of the ejecta layers had more expanded craters than the surrounding terrain. We extrapolate that the total volume of ice remaining within the entire ejecta deposit is as much as 74 km<sup>3</sup> or more. The variation in ice content between the ejecta layers could be the result of (1) volatile preservation from the formation of the DLE crater, (2) post-impact deposition in the form of ice lenses; or (3) preferential accumulation or preservation of subsequent snowfall. We have ruled out (2) as the primary mode for ice deposition in this location based on inconsistencies with our observations, though it may operate in concert with other processes. Although none of the existing DLE formation hypotheses are completely consistent with our observations, which may merit a new or modified mechanism, we can conclude that DLE craters contain a significant quantity of excess ice today.

© 2016 Elsevier Inc. All rights reserved.

### 1. Introduction

Impact craters can act as windows into planetary surfaces to provide insights about material properties. On Mars, the morphological characteristics of primary craters, including interior and ejecta traits, are known to vary with location, and particularly correlate with latitude and differing subsurface volatile content (e.g. Mouginiis-Mark, 1979; Barlow and Bradley, 1990; Barlow et al., 2001; Barlow, 2015; Jones and Osinski, 2015; Li et al., 2015). Here, we focus on double-layer ejecta morphology, which has long been associated with the presence of subsurface volatiles such as water ice.

Secondary craters can similarly provide information about the properties of planetary surfaces and shallow subsurfaces. Since

secondary craters from a particular impact form nearly simultaneously, morphological variations within a single secondary crater field can offer a broader understanding of the variations in the initial surface and near-surface properties across large regions. One example is thermokarstic alteration (expansion) of secondary craters, which involves the sublimation of impact-exposed excess ice in the shallow subsurface (Viola et al., 2015; Dundas et al., 2015).

#### 1.1. Double-layer ejecta craters

Layered ejecta deposits are common on Mars, and their morphologies suggest formation by fluidization of ground-hugging flows. In fact, most fresh craters greater than 5 km in diameter are surrounded by these fluidized ejecta deposits (Barlow, 2005). Layered ejecta deposits can be divided into three types: single-layer, double-layer, and multiple-layer ejecta (SLE, DLE, and MLE, respectively). SLE and MLE craters are thought to form in similar ways based on morphological characteristics, where MLE craters

\* Corresponding author at: Planetary Sciences, 1629 E. University Blvd, Rm. 324, Tucson, AZ, 85721.

E-mail address: [dviola@lpl.arizona.edu](mailto:dviola@lpl.arizona.edu) (D. Viola).

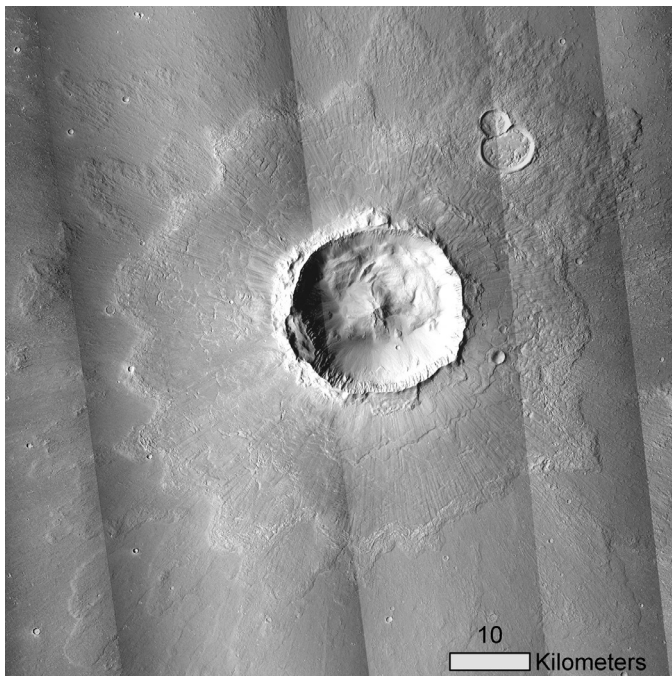


**Fig. 1.** An example of a well-preserved double-layer ejecta crater, Bacolor crater, located at 33°N, 242°E with a diameter of 20 km using images from CTX (P17\_007752\_2140\_XN\_34N242W; P21\_00904\_2132\_XN\_33N241W; P22\_009677\_2133\_XN\_33N241W; G22\_026674\_2133\_XN\_33N242W; G22\_026819\_2155\_XN\_35N241W; D04\_028718\_2124\_XN\_32N240W).

tend to be larger than SLE craters (e.g. Boyce and Mouginis-Mark, 2006). However, DLE craters, with two distinct layers of ejecta, are more enigmatic. Recently, DLE craters have been divided into two different groups: type 1 and type 2 (Barlow, 2015). Type 2 DLE craters have ejecta deposits with thin, sinuous layers that end in low ramparts, which are more similar to SLE and MLE craters and likely form in a similar fashion (Barlow, 2015). However, much of the previous research on DLE craters has focused on the more common Type 1 DLE craters, which account for >70% of the DLE craters in the northern hemisphere of Mars (Barlow, 2015). Type 1 DLE craters are typically characterized by a thicker inner ejecta layer with an annular moat outside of the crater rim and a rampart at the outer edge of the inner ejecta (Boyce and Mouginis-Mark, 2006), along with a thinner, more sinuous outer ejecta layer (Barlow, 1994) which also terminates in a low rampart. Bacolor crater, shown in Fig. 1, is a well-preserved example of this type of DLE crater. Two parameters are used to quantify these lobate ejecta morphologies: the extent of the fluidized ejecta (ejecta mobility, or EM, ratio) and the sinuosity of the ejecta layer (lobateness, or  $\Gamma$ ). EM is the ratio of the distance traveled by the ejecta to the crater radius, so higher values represent longer ejecta runout distances. Lobateness, defined by the equation below, takes into account the perimeter ( $P$ ) and area ( $A$ ) of an ejecta deposit, where  $\Gamma = 1$  is a circular deposit and higher values have increasingly sinuous ejecta edges.

$$\Gamma = \frac{P}{(4\pi A)^{1/2}}$$

For type 1 DLE craters, the median values of ejecta mobility and lobateness for the inner ejecta layer are 1.4 and 1.11, respectively. For the outer ejecta layer, the median values for ejecta mobility and lobateness are 3.1 and 1.15, respectively (Barlow, 2015). This shows that, in general, the inner ejecta layer of a type 1 DLE craters is more circular than its outer layer, and that the outer

ejecta layer generally travels about twice as far as the inner ejecta layer.

A system of radial grooves superposed on the innermost ejecta layer has also commonly been cited as a characteristic of DLE craters (e.g. Carr et al., 1977; Schultz and Gault, 1979; Mouginis-Mark, 1981; Boyce and Mouginis-Mark, 2006; Weiss and Head, 2013; Wulf and Kenkmann, 2015). However, the survey conducted by Barlow (2015) found that only 27% of both Type 1 and Type 2 DLE craters possess this feature, and that the radial texture is more common in DLE craters at lower latitudes. It is possible that the radial texture is less likely to form at higher latitudes, or that it tends to be rapidly erased by post-impact processes in these regions. The inner ejecta is generally thought to superpose the outer ejecta, suggesting sequential formation where the outer layer was emplaced first (Carr et al., 1977; Schultz, 1992; Barlow and Perez, 2003; Osinski et al., 2011). However, the opposite case, where the inner ejecta layer is emplaced first, has also been argued based on apparent radial grooves spanning both ejecta layers (Mouginis-Mark, 1981; Boyce and Mouginis-Mark, 2006).

DLE craters are preferentially found in mid- to high-latitude regions on Mars, and tend to have diameters of less than 50 km (Barlow and Bradley, 1990). These morphologies are broadly found in two latitude bands, between 30–50°S and 25–60°N (Boyce and Mouginis-Mark, 2006), although they are most abundant in the northern plains of Mars, including Arcadia, Utopia and Acidalia Planitiae (Barlow and Perez, 2003). This distribution of DLE craters correlates with areas of high water content as detected by the Gamma Ray/Neutron Spectrometer (Boynton et al., 2002; Barlow and Perez, 2003). Therefore, it is generally thought that the presence of ground ice plays a role in the formation of DLE craters. It is also interesting that DLE craters are often located in regions that contain SLE and MLE-type craters of about the same size and age (Barlow, 2005; Boyce and Mouginis-Mark, 2006), which has implications for the local and regional factors that influence ejecta fluidization.

Some work has been done to characterize the thermal properties of lobate ejecta deposits. Christensen et al. (2003) found that lobate ejecta morphologies can have different thermal properties between ejecta layers, although there is some variation that may be due to differences in emplacement or post-impact modification. There have been multiple subsequent observations of DLE craters using THEMIS nighttime IR to characterize particle sizes and thermal inertia. Baratoux et al. (2005) observed that, in particular, the distal edges of lobate ejecta deposits of SLE and DLE craters in Syrtis Major tend to be brighter in nighttime IR. Their observations were inconsistent with post-impact dust mantling or removal, suggesting that the observed thermal properties are controlled by the initial ejecta particle size distribution, where the edges of ejecta flows are most likely comprised of larger particles. A mechanism of “kinetic sieving” (Middleton, 1970) was proposed to explain this observation, where smaller particles tend to percolate downward in a flow while larger particles accumulate at the top of the flow and fall out closer to the flow front (Baratoux et al., 2005). Observations of another DLE crater found that the inner ejecta layer was warmer, and concluded that this layer must have a higher thermal inertia and be composed of coarser-grained materials (Komatsu et al., 2007). HiRISE observations of Steinheim crater revealed that the inner ejecta contains clusters of coarser material with radial orientations found close to the crater, whereas the outer ejecta layer tends to have blocky material towards the distal edges (Wulf et al., 2013). A survey including 12 DLE craters in Chryse Planitia observed in THEMIS nighttime IR claims to reveal an inconsistent trend, where 5 DLE craters were “inversely graded” (transitioning from fine-grained to coarse-grained materials with increasing distance from the crater), 3 DLE craters displayed the opposite pattern, and 4 DLE craters had no discernible trend in particle size

(Jones et al., 2016). However, it is possible that some of the DLE craters used in this study have been misclassified (Robbins and Hynek, 2012).

Several mechanisms have been proposed to explain the formation of DLE craters on Mars, based largely on the presence of volatiles and/or an atmosphere. It is, however, worth noting that DLE-like craters have also been identified on Ganymede and possibly Europa (Boyce et al., 2010), which may indicate an ejecta fluidization mechanism that is similar to the martian DLE craters. This suggests that an atmosphere is not necessary for this type of fluidization. In addition, layered ejecta has recently been proposed for some craters on Mercury (Xiao and Komatsu, 2013), although it is possible that these are the result of mass wasting rather than ejecta emplacement. Furthermore, the apparent lack of DLE craters on other ice-rich worlds like Enceladus may indicate that the presence of subsurface volatiles alone may not be sufficient for ejecta fluidization (Boyce et al., 2010).

The specific formation hypotheses that have been proposed for martian DLE craters are described below:

**Atmospheric effects:** Since layered ejecta patterns had not been found on bodies like the Moon or Mercury, it was originally proposed that the presence of an atmosphere, including atmospheric drag effects, may play a key role in the impact cratering and ejecta emplacement processes (Schultz and Gault, 1979). Interactions between the ejecta curtain and atmospheric vortices in particular have been cited as a possible explanation for the double-layer ejecta morphology. Experimental and numerical techniques have been used to observe the interaction between the ejecta curtain and the atmosphere and to determine the ejecta entrainment capacity of impact-generated winds under various atmospheric conditions (Barnouin-Jha et al., 1999a,b). Laboratory experiments demonstrated that ejecta patterns vary as a function of atmospheric pressure, and that lobate ejecta flows terminating in distal ramparts (including those with two layers of ejecta) can be produced when fine-grained material is entrained in turbulent atmospheric eddies that flow outward behind the ejecta curtain, scouring over the initial ejecta deposits and being deposited in long run-out flows (Schultz, 1992). This formation mechanism is generally independent of the presence of water, although volatiles can increase the run-out distance of the ejecta. However, HiRISE images clearly show boulders in the layered ejecta deposits (e.g., Wulf et al., 2013), so the ejecta is not entirely fine-grained materials entrained by atmospheric eddies.

**Presence of volatiles/base surge hypothesis:** Surfaces with varying volatile content and possible subsurface layering could lead to the formation of layered ejecta. Since DLE craters are commonly found in locations with periglacial features, Mouginiis-Mark (1981) proposed a formation mechanism where an impact excavates through a dry upper layer into a volatile-rich layer underneath. In this model, the inner ejecta layer would first form from the uppermost dry material, and the more mobile, volatile-rich ejecta plume would collapse and scour over the inner ejecta layer, creating the radial grooves before being deposited farther away as the outer ejecta layer. The base surge hypothesis, a two-step mechanism proposed by Boyce and Mouginiis-Mark (2006), builds on this idea by incorporating additional details. The updated model states that the emplacement of the inner ejecta layer is similar to that of single-layered ejecta (SLE) craters and likely involves a ballistic and/or flow process. An impact-generated explosion column similar to those generated in volatile-rich explosive volcanism then collapses in a base surge of lofted fine-grained material, creating the outer ejecta that flows over and etches radial patterns into the inner ejecta before being deposited. This model would suggest that the bulk of the inner ejecta is comprised of dry materials, and if any volatiles were deposited with the base surge, they would more likely be found in the outer ejecta.

**Impact melt and melting of ground ice:** Early work first suggested that impact melting of ground ice may play a role in the formation of layered ejecta patterns (Carr et al., 1977). Wohletz and Sheridan (1983) demonstrated experimentally that ejecta emplacement is strongly controlled by the mass ratio of water to impact melt, and therefore developed a conceptual model that invokes both impact melt and subsurface water. Their observations found that, when the mass ratio of water to impact melt is  $>0.2$ , the corresponding increase in vapor expansion upon impact results in the fluidization and longer ejecta runout distances that are characteristic of rampart ejecta morphologies (Wohletz and Sheridan, 1983). In the case of craters with more than one ejecta layer, they state that outer ejecta layers can be ballistically-deposited, driven by inertia, whereas the inner ejecta layer is deposited as a water-rich, viscously-driven flow. Osinski (2006) also proposed that the driving factors of ejecta fluidization are subsurface volatile content and impact melt. This model argues that, during the crater excavation stage, the outer ejecta is first deposited ballistically, and the inner ejecta is subsequently deposited as a ground-hugging flow comprised of overflowing impact melt during the modification stage as the central peak is uplifted. Osinski (2006) further suggested that additional ground-hugging flows can lead to the multiple layered ejecta patterns also observed on Mars, where the degree of ejecta fluidization depends on the amount of ground ice melting that takes place. Osinski's arguments were supplemented by observations of terrestrial impact craters, Haughton and Ries, where he suggested that they appear to have formed in two episodes akin to martian DLE craters. However, numerical models have demonstrated that, at least in the case of Ries crater, this formation mechanism may be unlikely (Artemieva et al., 2013).

**Ballistic sedimentation:** Commonly attributed to the formation of continuous ejecta on the Moon, ballistic sedimentation involves ejecta particles that can mobilize "secondary ejecta" as they impact the surface, integrating pre-existing surface materials into the final ejecta deposit (Oberbeck, 1975). In the case of layered terrains containing some fraction of subsurface ice, as is expected for regions of Mars during different points in the planet's obliquity cycle, it is possible for ballistic sedimentation to incorporate this subsurface ice to produce ejecta blankets with layered patterns such as the SLE, DLE, and MLE craters observed on Mars (Oberbeck, 2009). Furthermore, Oberbeck (2009) suggested that water/ice could have locally comprised up to  $\sim 21\%$  of the subsurface between 0.27 and 2.5 km in depth.

**Combination effects:** Some combination of volatiles and an atmosphere has also been suggested to explain the formation of DLE craters and the other layered ejecta types (e.g. Barlow, 2005). Komatsu et al. (2007) proposed a more detailed combination mechanism, where the inner ejecta layer forms by ballistic emplacement and water-rich ground-hugging flows, with possible influences from atmospheric interactions. The outer ejecta forms from a combination of three processes largely driven by impact-generated shockwaves and winds: (1) near-surface sediment liquifaction, (2) water-rich ballistic emplacement, and (3) atmospheric vortices and/or base surges. The relative significance of each of these mechanisms on the final ejecta morphology may be driven by variations in surface and impact properties.

**Granular flow:** The model of Wada and Barnouin-Jha (2006) has suggested that neither volatiles nor an atmosphere are required to initiate flow as a dry granular medium to produce the fluidized morphology of martian crater ejecta. This formation mechanism would be independent of the presence of volatiles. However, while this model demonstrated evidence for flow, it failed to produce the layered ejecta patterns commonly observed on Mars, including common characteristics of DLE craters such as terminal ramparts and annular depressions around the crater rim.

**Subsurface and surface icy layers:** Model simulations of impacts into surface and subsurface icy layers reveal interesting variations in crater and ejecta morphologies due to the strength differences between rock and ice (Senft and Stewart, 2008). In the case of an impact into a surface with a buried ice layer, a thick inner region of ejecta and a thin outer region were produced, similar to the layers observed in martian DLE craters (Senft and Stewart, 2008).

Weiss and Head (2013) proposed that DLE craters could be formed by an impact directly into a snow/ice substrate, where the inner layer is actually produced when material overlying the ice near the crater rim landslides downslope shortly after impact. This would expose some of the ice, which would be expected to subsequently sublimate. This glacial substrate model requires surficial ice deposits present at the time of DLE-crater formation, and relies on the history of glaciation in the martian past, where glacial deposition can be correlated with obliquity-driven changes in the climate (Laskar et al., 2004; Dickson et al., 2008). The glacial substrate model suggests that some of the initial ice/snow layer remains preserved beneath the crater ejecta, and that the ejecta protected the ice from subsequent climate shifts that led to widespread volatile loss across the broader regions where they are found. It has been demonstrated that thicker ejecta deposits ( $\geq 10$  m) are more capable of inhibiting ice sublimation than thinner deposits over timescales of tens of millions of years under present surface temperatures (Black and Stewart, 2008), which would suggest that more ice may be preserved by the thicker inner ejecta deposits. However, Senft and Stewart (2008) also modeled the case of an impact into a surface ice layer and did not observe the distinct ejecta layering that was seen in the case of a buried ice layer, although this model does not account for post-impact modification of the ejecta deposits (such as landsliding events).

**Other landslide effects:** It has also been argued that landslide effects can produce DLE morphology in the absence of a significant deposit of ice at the surface. Wulf and Kenkmann (2015) propose that an impact into a rock/ice mixture can produce high ejection angles and a water-rich ejecta curtain due to shock-induced vaporization and melting of ice. The vaporization and melting produces the outer ejecta as a liquid-rich debris avalanche or debris flow. High ejection angles would lead to thicker proximal ejecta deposits, which can produce the inner ejecta layer in a translational slide driven by basal melting. This hypothesis suggests that there would initially be high water content in the outer ejecta, and lower water content in the inner ejecta.

### 1.2. Expanded secondary craters

Expanded craters, shown in Fig. 2, are commonly found in Arcadia Planitia and the plains north of Alba Mons, in the northern mid-latitudes of Mars (Viola et al., 2015). These unique craters lack extant rims and have a central crater bowl surrounded by a shallow extension to the surrounding surface such that their diameters appear to have increased. The expansion of these craters is most likely related to the presence of excess subsurface ice. In contrast to pore ice that only fills regolith pore spaces, “excess” ice is that which exceeds the available regolith pore space, and it is generally comprised of relatively pure water ice. Possible formation mechanisms for excess ice on Mars include the deposition and burial of glaciers or snowfall (Levrard et al., 2004; Schorghofer and Forget, 2012), the growth of ice lenses via groundwater migration (Sizemore et al., 2015), or periodic temperature cycles leading to thermal cracking and water vapor diffusion to build up extensive ice deposits (Fisher, 2005). Excess ice can be broadly found in the martian northern mid- to high-latitudes as low as  $38^\circ\text{N}$ , and has been identified by multiple instruments and observations. These include data from the Neutron Spectrometer

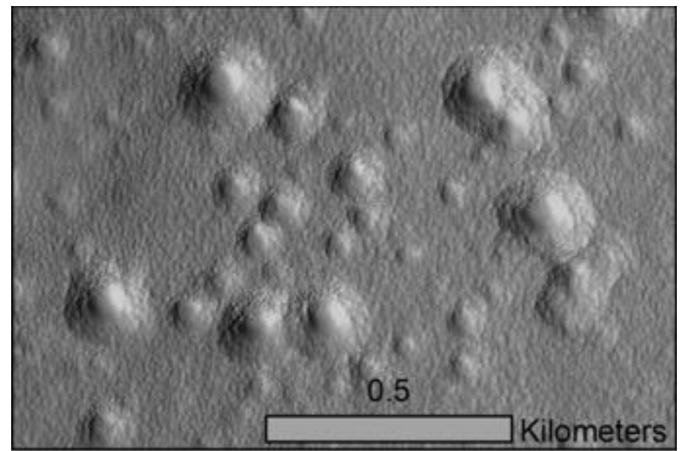
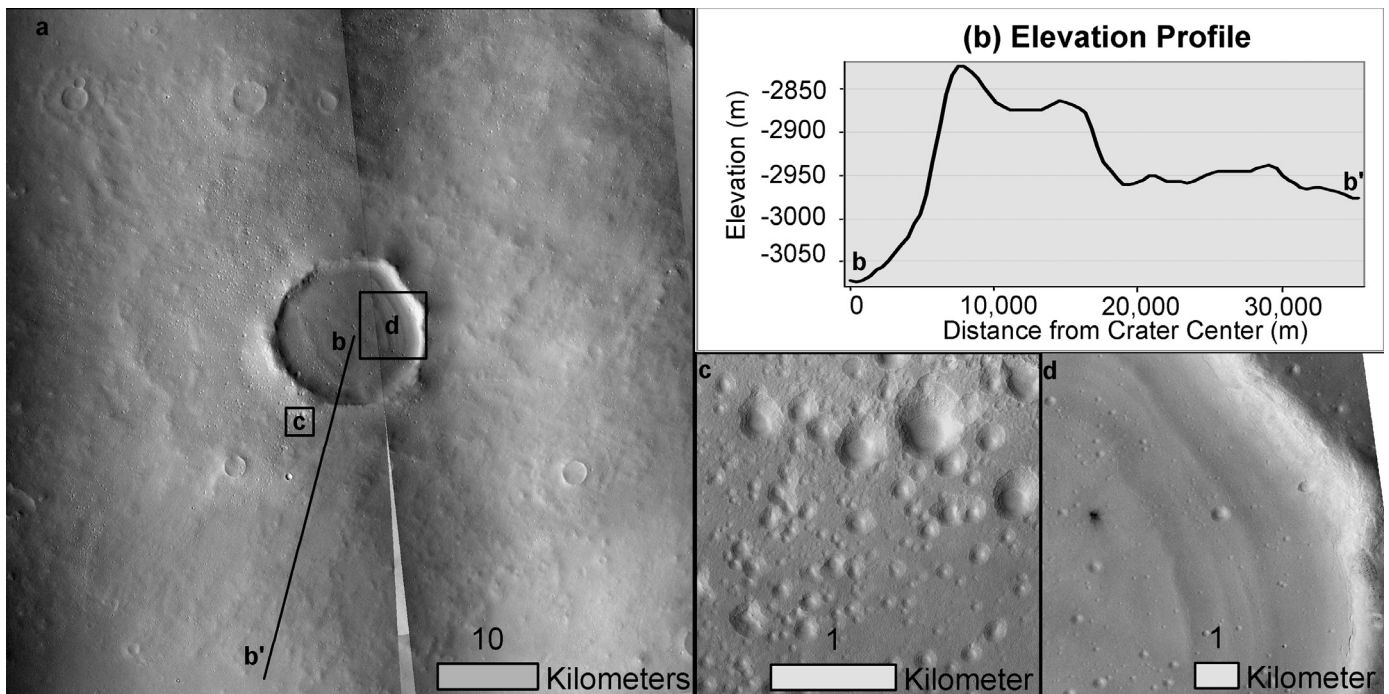


Fig. 2. Expanded secondary craters in ESP\_017875\_2305, centered near  $50.2^\circ\text{N}$ ,  $219.1^\circ\text{E}$ . Illumination direction is from the left.

onboard Mars Odyssey (e.g. Boynton et al., 2002; Feldman et al., 2004), the Thermal Emission Spectrometer (TES) on Mars Global Surveyor (Bandfield and Feldman, 2011), the Mars Advanced Radar for Subsurface and Ionosphere Sounding (MARSIS) on Mars Express (Mouginot et al., 2010, 2012), the Shallow Radar (SHARAD) instrument on the Mars Reconnaissance Orbiter (MRO) (Holt et al., 2008; Plaut et al., 2009; Bramson et al., 2015), the Phoenix lander (Smith et al., 2009; Mellon et al., 2009), and recent mid- to high-latitude impact craters that expose clean ice (Byrne et al., 2009; Dundas et al., 2014). Excess ice is also likely at high latitudes in the southern hemisphere based on Neutron Spectrometer data (Boynton et al., 2002) and observations of thermokarstic features like scalloped terrains found poleward of  $\sim 50^\circ\text{S}$  (Zanetti et al., 2010), although few ice-exposing impacts have been observed in the southern hemisphere due to observational limitations (Dundas et al., 2014).

Crater expansion is thought to be thermokarstic in nature. On Earth, “thermokarst” is traditionally associated with collapse features resulting from the phase transition between ice and liquid water. However, since liquid water is highly unstable on Mars, in this case, we consider “sublimation thermokarst”, which results from the transition from ice to water vapor. Throughout this paper, the term “thermokarst” will refer to *sublimation* thermokarst. Thermokarstic crater expansion, then, is thought to occur when an impact exposes a subsurface excess ice layer to the atmosphere. Since water ice is not stable when directly exposed to the martian atmospheric pressure, the impact-exposed ice sublimates over time, and the overlying dry material, including the once-extant crater rim, will collapse into the expanding crater. This effect has been demonstrated theoretically using thermal and landscape evolution models to simulate impacts into relatively clean ice (Dundas et al., 2015): over time, craters grow wider in diameter and become shallower, with elevation profiles comparable to those observed in Arcadia Planitia. Expansion likely ceases when enough material has accumulated over the excess ice to shelter it from further sublimation. Excess ice is key to the expansion process, since the loss of pore-filling ice would not result in this type of thermokarstic process, as demonstrated in Dundas et al. (2015). Expanded craters likely require the presence of a deposit of excess ice with a thickness that is, at minimum, comparable to or somewhat less than the depth of the craters. However, expansion can occur from a variety of geometries, so the detailed implications for ice stratigraphy and thickness are not certain (Dundas et al., 2015).

Since the widespread loss of excess ice by terrain dissection would also result in the loss of the surface expanded craters,



**Fig. 3.** (a) CTX coverage of the study double-layer ejecta crater. The inner ejecta layer lies within about 2.5 crater radii, and the outer layer extends to approximately 5 crater radii. The rim of a neighboring crater can be seen in the upper right of the image. (b) Elevation profile from the center of the crater to the surrounding terrain, showing the moat near the crater rim and the ramparts at the edge of each ejecta layer. (c) HiRISE subset of expanded craters on the inner ejecta layer of the DLE crater. (d) CTX close-up of concentric crater fill with some expanded craters and a dark-colored new small impact crater observed in the crater fill.

the modern presence of these thermokarstic features implies the presence of extensive excess ice throughout the broader region in which they are found. In Arcadia Planitia, where expanded craters are particularly abundant, these features are posited to be secondary craters based on their radial associations with several primary craters. Crater age dating estimates of these primary craters estimated that the ice sheet in Arcadia Planitia is at least tens of millions of years old (Viola et al., 2015), although these observations cannot constrain the upper limit on the age of the ice sheet. It is also important to note that extensive terrain dissection has been observed throughout much of the martian mid-latitudes (Mustard et al., 2001) and presents evidence for climate change, consistent with the obliquity fluctuations that Mars has experienced on timescales of  $\sim 100,000$  years (Laskar et al., 2004). Arcadia Planitia, however, is a notable mid-latitude exception to the observed trends in terrain dissection. While it is not entirely clear why this is the case, it offers additional evidence for the long-term preservation of subsurface excess ice within this region on timescales that greatly exceed fluctuations in the martian climate.

In this study, we have identified a DLE crater with secondaries superposed on it, many of which show evidence for thermokarstic expansion and are part of the secondary crater fields identified in Viola et al. (2015). The differences in the expansion morphology of these overlying secondaries can be used to infer the properties of the two ejecta layers as well as in the surrounding terrain, and offer constraints on the amount of ice present today and at the time of secondary crater formation.

## 2. Study area

This work focuses on a 15-km DLE crater in Arcadia Planitia, centered at  $50.4^{\circ}\text{N}$ ,  $219.6^{\circ}\text{E}$  (Fig. 3), which contains abundant superposed expanded secondary craters (Fig. 3c). The crater is found within the late Hesperian lowlands (IH1) unit identified by Tanaka

et al. (2014). It has a sharp crater rim, with an annular depression outside the rim and a rampart at the outer edge of the inner ejecta layer, all of which are characteristic of double-layer ejecta craters and can be seen in the elevation profile in Fig. 3b. The crater also appears to have superposed the ejecta of a 30-km SLE crater that lies to the northeast, such that the ejecta of the 15-km DLE crater seems shortened in that direction. The lobateness for the inner and outer ejecta layers is 1.6 and 1.92, respectively (Robbins and Hynek, 2012). These values indicate that there is an inherent non-circularity to the ejecta layers and that the outer layer is more sinuous than the inner layer. This is consistent with the characteristics of Type 1 DLE craters (Barlow, 2015). However, the inner ejecta layer has a lobateness that appears anomalously high compared to typical DLE craters, which have values that are typically in the range of 1.03–1.31 with a median value of 1.11 (Barlow, 2015). This may be related to the fact that the inner ejecta layer is noticeably asymmetric where it superposes the ejecta of the nearby 30-km crater.

There is no radial groove pattern identifiable on the inner ejecta. However, as noted previously, this is not necessarily a prerequisite feature of DLE craters. Furthermore, the surface of the crater and ejecta is covered with small, mostly secondary, craters, and has undergone some degree of periglacial alteration that may have contributed to the erosion of some of the primary crater's original characteristics. The source of the overlying secondary craters is not entirely apparent and it is possible that they were produced by multiple impacts, although the degree of degradation and expansion for most of the secondaries appears to be similar, suggesting a common source. Likely candidate source craters include Gan crater ( $61.7^{\circ}\text{N}$ ,  $229^{\circ}\text{E}$ ;  $D = 19$  km) and Domoni crater ( $51.4^{\circ}\text{N}$ ,  $234.4^{\circ}\text{E}$ ;  $D = 14$  km), both situated to the northeast of the study DLE crater and consistent with the general northeast-to-southwest orientation of the secondary crater ray. In either case, these two potential source craters are likely on the order of tens

of millions of years old ( $\sim 70$  Myr old in the case of Gan crater; Viola et al., 2015), and the presence of these secondaries superposed on the study DLE crater indicates that the DLE crater must pre-date the source crater of the secondaries. It is worth noting, however, that we cannot rule out the possibility that the secondaries were sourced from a more distant, unidentified impact event of uncertain age.

The DLE crater is approximately 400 m deep, and has a depth-to-diameter ( $d/D$ ) ratio of  $\sim 0.027$ . This  $d/D$  ratio is low compared to the commonly accepted values for fresh, complex impact craters (Pike, 1980; Garvin and Frawley, 1998), even when accounting for latitudinal variations in fresh crater depths (Mouginis-Mark and Hayashi, 1993; Stepinski et al., 2009; Robbins and Hynes, 2012). However, crater-filling material is apparent within the crater, which alters the depth-to-diameter ratio. Expanded secondary craters are found within this infilling material, and the regions that are not heavily covered in craters contain concentric lineations similar in appearance to concentric crater fill (Fig. 3d). Concentric crater fill (CCF) has been connected to glacial activity (Levy et al., 2010), so both of these observations offer indirect evidence for the presence of ice in the infilling material. The ice-rich nature of the infilling material was confirmed by a small, new impact crater that was observed in CTX image G21\_026446\_2327\_XN\_52N141W\_120318 (shown in Fig. 3d) and bright material likely to be exposed ice was found in follow-up HiRISE image ESP\_026802\_2305 (Dundas et al., 2014). If we assume that the change in crater depth over time is due only to the ice-rich infilling material, we can acquire constraints on the maximum depth of ice preserved in the crater today. This further requires an assumption on the initial crater  $d/D$  ratio. If the initial  $d/D$  ratio was similar to the estimated global range of 0.05–0.18 for complex craters (Pike, 1980), then the initial crater depth would have been between 0.75–2.7 km deep. This would suggest that between 350 m and 2.3 km of infilling material was deposited and remains today if all of the change in depth is due to infilling processes, although it is likely that there has also been some erosion of the rim over time. Garvin and Frawley (1998) proposed a diameter-dependent equation for  $d/D$  ratio, where depth is proportional to  $D^{0.49}$  for complex craters, which would suggest that the initial depth of a 15-km crater would be 942 m, indicating that up to 540 m of infilling material was deposited in the crater. If we use the relationships derived by Robbins and Hynes (2012) for fresh, complex craters in the northern plains, the initial depth would have been 1065 m. This indicates that up to 665 m of fill is present in the crater today, given the same assumption that the present depth is solely the result of infilling. This is well within the bounds expected from Pike (1980): either way, the DLE crater likely contains as much as several hundred meters of icy infill, although other erosional processes may have contributed to the shallowing of the crater.

Fig. 4 shows THEMIS nighttime IR of the study DLE crater, where red indicates higher temperatures and blue represents lower temperatures. Most of the area covered by the HiRISE DTMs of interest (which are described in the next section) is fairly uniform and dark in IR, suggesting more fine-grained materials without large variations between the ejecta layers. There are some brighter, warmer regions at the distal edge of the outer ejecta layer, as well as a region of the inner ejecta to the north of the crater, that appear to have higher rock abundances or rougher surface textures. However, the overall appearance of more fine-grained materials is in contrast to the observations described above. This may be due to post-impact processes, since the primary crater itself is on the order of  $>$ tens of millions of years old. For example, it is possible that the initially-rougher inner ejecta could have trapped more dust (and ice) than the outer ejecta, leading to the overall equalizing of the particle sizes that we observe.

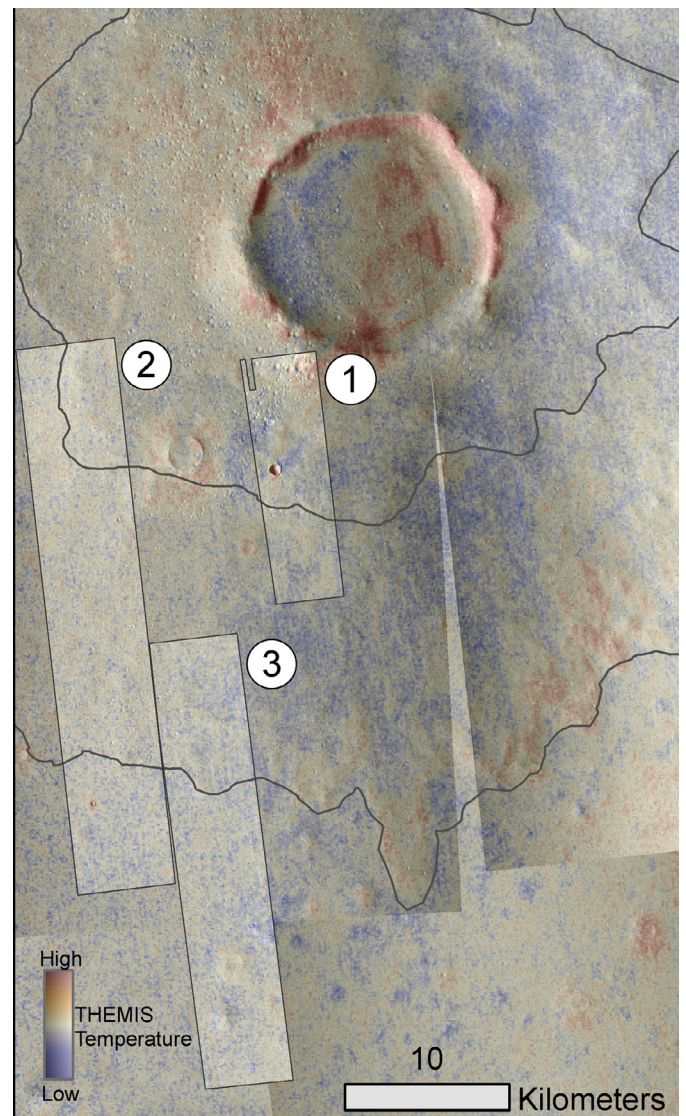


Fig. 4. DLE crater with nighttime THEMIS IR overlay. Red indicates higher temperatures, and blue indicates cooler temperatures. The outer ejecta shows warmer temperatures towards the distal edges in the right part of the figure and around the crater rim. These regions may have higher rock abundances or rougher surface materials. The DTM locations (shown as footprints; numbers correspond to HiRISE stereo pairs listed in Table 1) are largely uniform and low in temperature, with the exception of very close to the crater rim and a couple of smaller primary craters. Background CTX images are: B20\_017308\_2313\_XN\_51N140W, B21\_018007\_2306\_XN\_50N140W, and G22\_026802\_2283\_XI\_48N139W. (For interpretation of the references to colour in this figure legend, the reader is referred to the web version of this article.)

### 3. Objective

A preliminary “case study” of a sampling of expanded secondaries overlying this 15-km DLE crater found that there is a dichotomy in the crater diameters between the inner and outer ejecta layers (Viola et al., 2015). This initial work was done using a single Digital Terrain Model (DTM) from the High Resolution Imaging Science Experiment (HiRISE) on MRO, made from stereo pair ESP\_027158\_2305/ESP\_026446\_2305 and which spans only the two ejecta layers. The present study builds upon that work by analyzing the same DTM and two additional HiRISE stereo pairs in greater detail, as we will describe. All DTMs were produced using SOCET Set and the methods described in Kirk et al. (2008), and have vertical precisions on the order of tens of centimeters. The additional

**Table 1**  
Summary of DTMs mapped.

	HiRISE stereo pair	Area (km <sup>2</sup> )	N (expanded)	N (non-expanded)	N (ambiguous)	Ejecta layer
1	ESP_027158_2305 and ESP_026446_2305	64.8	873	116	224	Inner, outer
2	ESP_017875_2305 and ESP_018007_2305	199.9	2095	997	1491	Inner, outer, surroundings
3	ESP_034384_2300 and ESP_033738_2300	147.3	1241	1394	2404	Outer, surroundings

**Table 2**  
Summary of the number of secondary craters of each morphology mapped in each region.

Location	Mapped area (km <sup>2</sup> )	N (expanded)	N (non-expanded)	N (ambiguous)
Inner ejecta	67.9	917 (80.5%)	34 (3.0%)	188 (16.5%)
Outer ejecta	195.6	2280 (55.1%)	585 (14.2%)	1269 (30.7%)
Surroundings	146.6	1012 (18.2%)	1888 (33.9%)	2662 (47.9%)

HiRISE stereo pairs are ESP\_017875\_2305/ESP\_018007\_2305, spanning the two ejecta layers and part of the surrounding terrain, and ESP\_034384\_2300/ESP\_033738\_2300, which spans the outer ejecta layer and the surroundings.

We provide a more accurate quantification of the ice loss during the secondary crater expansion process by using the volumes of expanded craters as a proxy for ice loss. This assumption was justified in Viola et al. (2015), where the crater cavities of non-expanded Zunil crater secondaries had volumes that were roughly the same as the total volume of their preserved rims and ejecta (to within a factor of 2). This can then be used as a means of estimating how much ice must be present within each ejecta layer and in the surrounding terrain in the present day. Clarifying the volatile composition of each ejecta layer has implications on the formation mechanism of martian DLE craters. We focus on a single DLE crater in this study because it is so densely covered by secondary craters and is well covered in HiRISE stereo imagery. However, it has been observed that expanded craters tend to be preferentially found on the ejecta and within the infilling material of older craters within the region of Arcadia Planitia (Viola et al., 2015), broadly suggesting that many craters have preserved excess ice (see also Section 4.5).

#### 4. Superposed secondary crater morphologies: distribution and parameters

All small craters within each DTM were approximated as ellipses using the Crater Helper Tools add-in for ArcGIS (Nava, 2011), and their geographic coordinates and planar parameters (major and minor axis diameters, eccentricity, azimuth) were measured. For non-overlapping craters, 3D parameters such as volume (described in Section 5), three-dimensional surface area, and depth were also measured. Depths were estimated from the average elevation at the edge of the crater and the elevation of the crater center, and were used to calculate d/D ratios.

Each crater was characterized as (1) expanded, non-expanded, or ambiguous; (2) overlapping or non-overlapping; and (3) primary crater or likely secondary crater. Since the focus of this study is thermokarstically-expanded secondary craters, a small number of suspected primary craters (as evidenced by sharper crater boundaries and the presence of a rim/ejecta) were removed from the data set. However, it is likely that there is some primary crater contamination within the data set if small primary craters in the region underwent sufficient erosion and/or thermokarstic expansion. The “ambiguous” designation was used to describe craters that did not clearly fit into either morphological category, either because they were too small to distinguish a type or they appeared too heavily degraded to be definitively classified. This could include craters that have been so modified by expansion that they lack distinctive morphologies.

A total of >10,800 secondary craters were mapped and classified in this study. Table 1 describes the three HiRISE DTMs used, in-

cluding the number of craters of each morphology mapped in each and a description of the regions that the DTM spans. Table 2 shows the numbers of craters with each morphology found in each region of interest: inner ejecta, outer ejecta, and surroundings.

##### 4.1. Geographic distribution and abundance of expanded craters

The geographic distribution of expanded, non-expanded, and ambiguous secondary craters can be seen in Fig. 5, where the boundaries between ejecta layers and the surrounding terrain are delineated. In addition to the overall distribution of the morphological types within the ejecta layers themselves, features of note include several hummocks in the surrounding terrain that are similar in appearance and texture to the ejecta layers and contain anomalous abundances of expanded craters suggestive of subsurface ice. Fig. 6 compares the different textures found in the study area, including the ejecta, the surrounding plains, a hummock within the plains, and the material that infilled the crater.

Fig. 7a compares the number of expanded and non-expanded craters in each region. The inner ejecta layer contains the highest percentage of expanded craters (96%), whereas the surrounding terrain contains the lowest percentage of expanded craters (35%). The outer ejecta also contained a high percentage of expanded craters (80%), although it was lower than that of the inner ejecta. This trend persists when craters with “ambiguous” morphologies are included, as shown in Fig. 7b. The percentage of expanded craters (relative to all superposed secondaries, including those with ambiguous morphologies) on the inner ejecta, outer ejecta, and surrounding terrain is 80%, 55%, and 18%, respectively.

##### 4.2. Size-frequency distributions

Size-frequency distributions (SFDs) of the mapped secondary craters in each region also demonstrate that, when considering all secondary craters, the SFD of the inner layer (which includes the highest percentage of expanded craters) is slightly shifted towards larger diameters at the same incremental frequencies (Fig. 8a), although there is some overlap between the inner and outer ejecta layers at the smaller crater bins. The same trend can be observed when only considering the expanded craters within each region, and expanded craters are shifted to much greater diameters when compared with non-expanded craters in both the outer ejecta and surrounding terrain (Fig. 8b), although there were not enough non-expanded secondaries on the inner ejecta to generate a meaningful SFD.

##### 4.3. Depth-to-diameter ratios

Fig. 9 shows the relationship between crater diameter and d/D ratio split by crater type for all non-overlapping craters (craters were binned in intervals spaced geometrically by a factor of 2<sup>1/8</sup>, where most bins except the largest and smallest contained >10

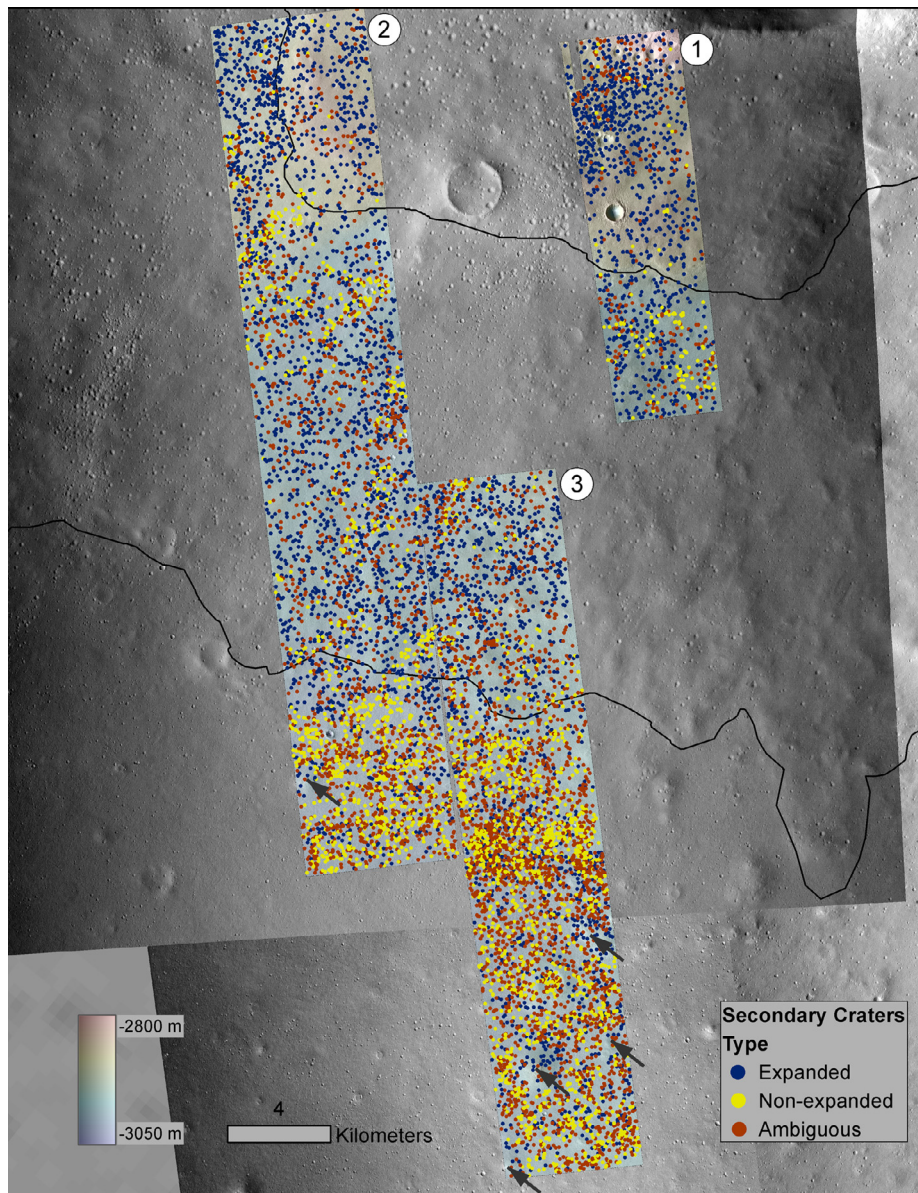


**Fig. 5.** The distribution of secondary craters mapped in the three HiRISE DTMs used in this study. The HiRISE DTMs, displayed in colorized elevation, are superposed on CTX images of the DLE crater. The numbers at the upper right of each DTM corresponds to the numbers in Table 1. The rim of the study DLE crater can be seen in the upper right. Dark blue points represent expanded craters, yellow points represent non-expanded craters, and red points represent craters with an ambiguous morphology. The inner and outer ejecta layers are delineated by black lines, and arrows indicate the locations of hummocks in the surrounding terrain (discussed in Section 4.4). (For interpretation of the references to colour in this figure legend, the reader is referred to the web version of this article.)

craters). Overlapping craters were not used for this analysis since overlaps lead to errors in the elevation of the crater edges (and therefore lead to erroneous depth measurements), so it is important to note that this does not account for some of the largest craters. The  $d/D$  ratio increases with binned diameter for both non-expanded and expanded secondary craters, and that the non-expanded craters have a steeper increase in this ratio.

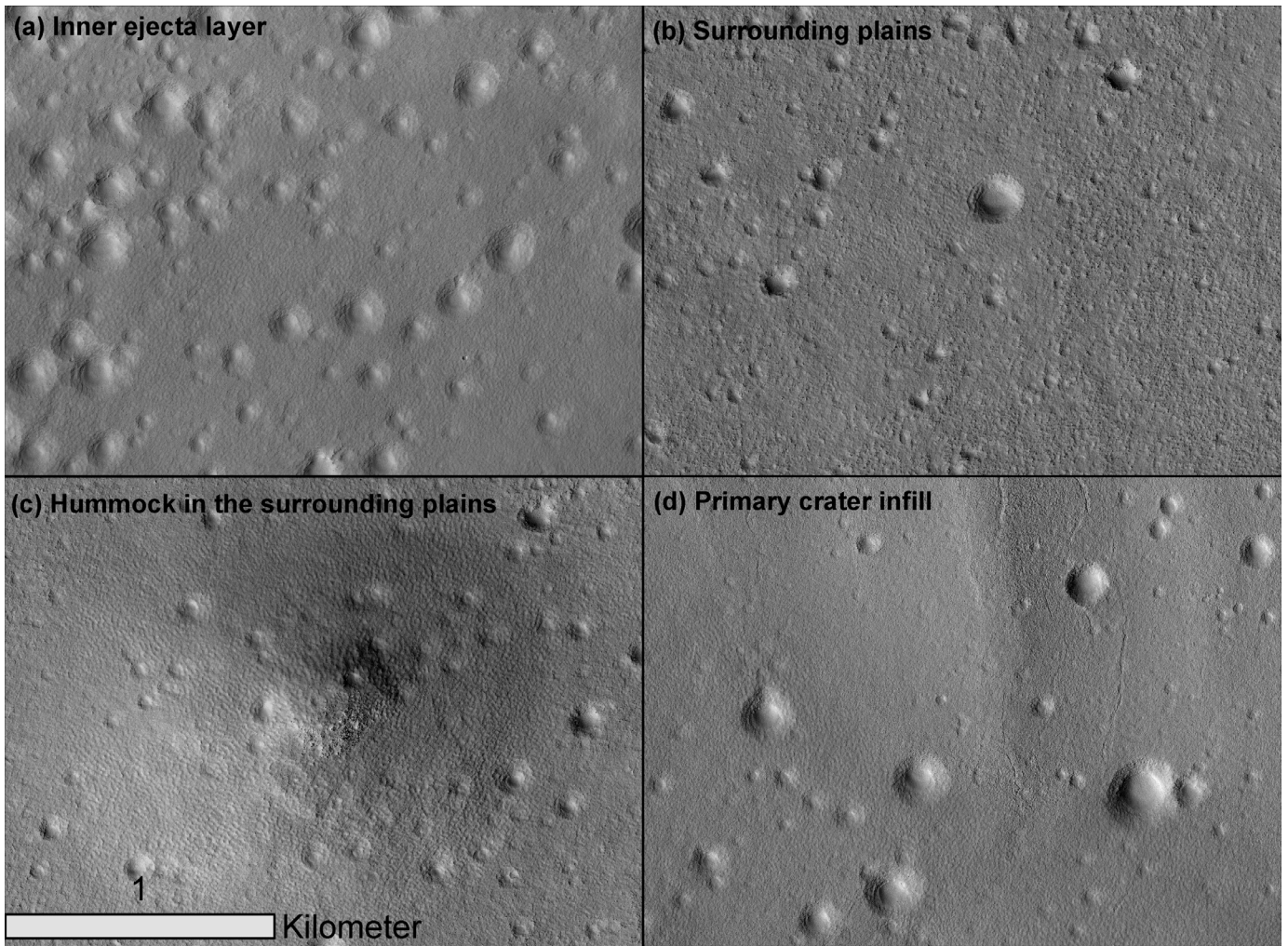
#### 4.4. Crater morphology and elevation

Fig. 5 reveals isolated hills that seem to preferentially contain expanded craters within the surrounding terrain (one such feature can be seen in Fig. 6c). There are also regions within the outer ejecta at lower elevations, even when accounting for the elevation of the ejecta itself, that seem to concentrate non-expanded craters. In the case of the outer ejecta, this may suggest localized ice loss or intrinsic variation in ejecta thickness in those re-

gions. The heights of the hummocks in the surroundings (as measured from HiRISE DTMs) are typically in the range of 11–25 m (the tallest is ~56 m high), and they are hundreds of meters in diameter. We infer that the hummocks contain ice based on the preferential presence of expanded craters.

#### 4.5. Evidence from additional DLE craters

We conducted a survey of primary craters throughout Arcadia Planitia in order to demonstrate the applicability of the detailed study of a single DLE crater to the broader population of DLE craters. Well-preserved primary craters with diameters greater than 5 km that lie within the Arcadia Planitia secondary crater fields mapped in Viola et al. (2015) were identified from the Robbins crater database (Robbins and Hynes, 2012), and some of the layered ejecta morphologies were updated to be consistent with the ejecta classifications described in Barlow (2015). We looked



**Fig. 6.** Textural differences between (a) the inner ejecta layer; (b) the surrounding plains; (c) one of the hummocks in the surrounding terrain; and (d) the primary crater infill. Note in particular the similarities between the ejecta and the hummocks.

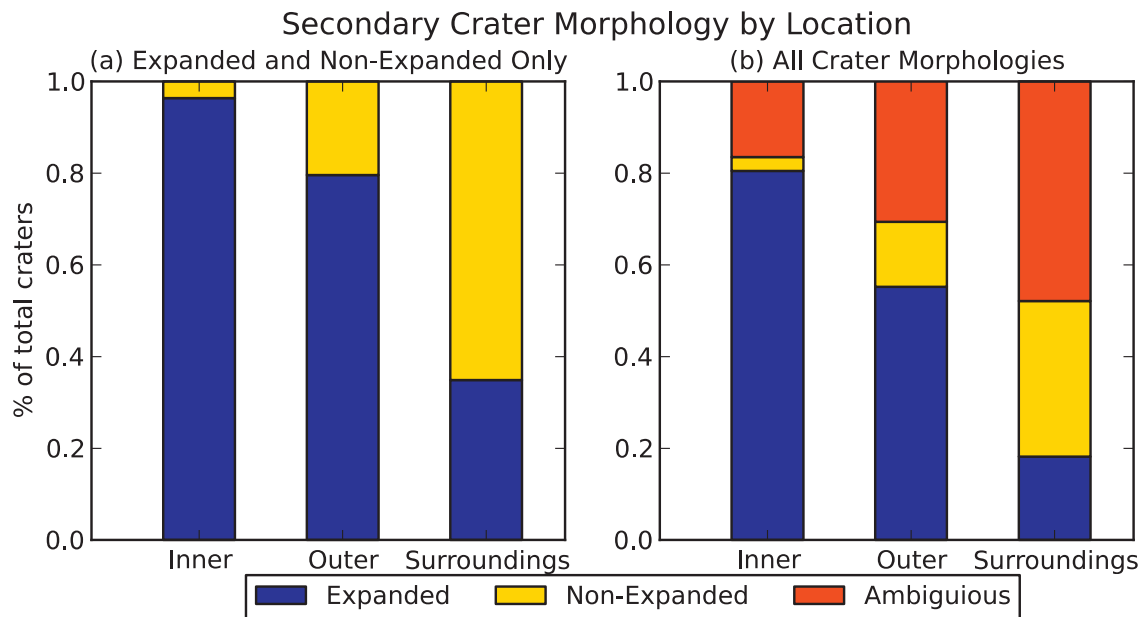


**Fig. 7.** (a) The percentage of expanded and non-expanded secondary craters mapped on the inner ejecta layer, outer ejecta layer, and surrounding terrain. The relative number of expanded craters is much greater on the inner ejecta layer, and decreases markedly in the surrounding plains. (b) Same as left, including secondary craters with "ambiguous" morphologies. It is still apparent that the percentage of expanded craters decreases as the location moves farther from the crater rim. (For interpretation of the references to colour in this figure legend, the reader is referred to the web version of this article.)

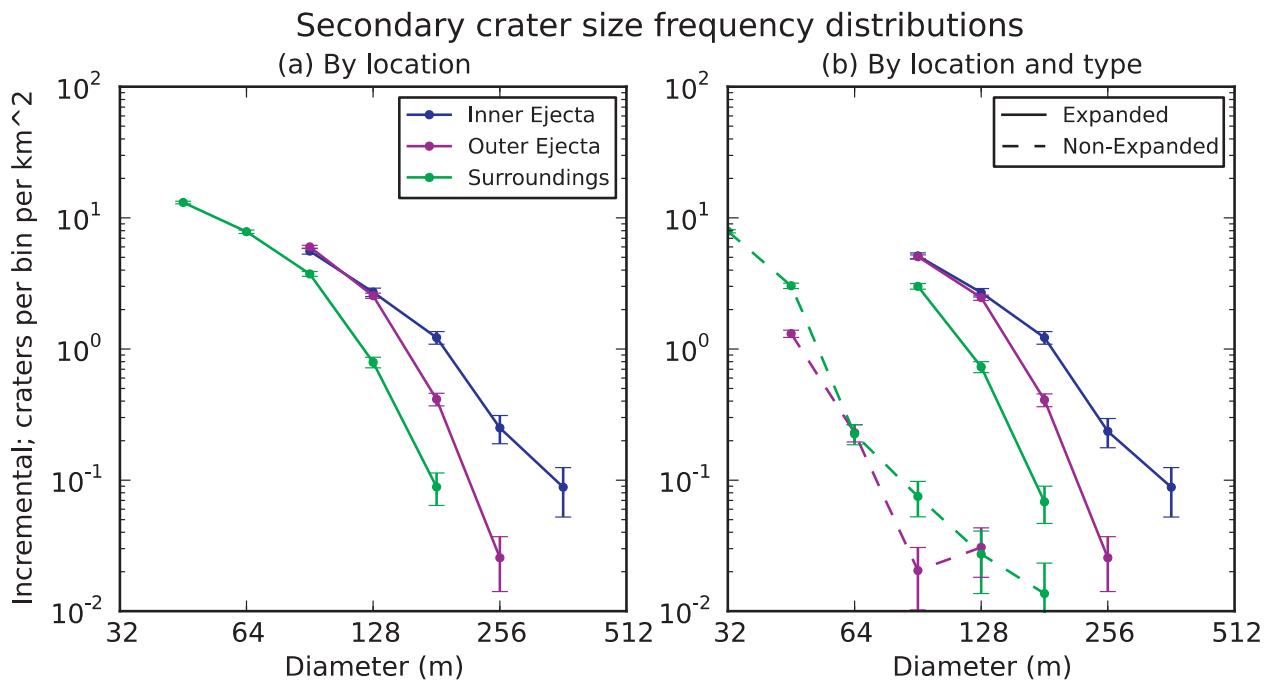


**Fig. 8.** (a) Log-incremental size-frequency distribution of all secondary craters overlying each region of interest: inner ejecta layer (navy), outer ejecta layer (purple), and surroundings (green). (b) Log-incremental size frequency distributions for expanded craters (solid lines) and non-expanded craters (dashed lines) in each region: navy=inner, purple=outer, green=surroundings. (Note: there were not enough non-expanded craters in the inner ejecta to produce meaningful results). Error bars are  $\sqrt{N}$  (per bin) normalized over the areas of interest. (For interpretation of the references to colour in this figure legend, the reader is referred to the web version of this article.)

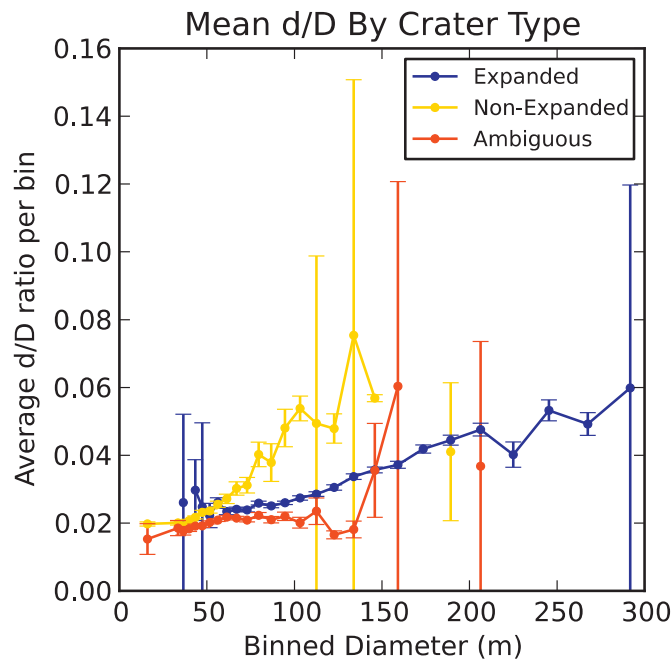


**Fig. 9.** Diameter-binned depth-to-diameter ratios for superposed secondary craters of each type.  $d/D$  ratio increases with increasing diameter for both expanded and non-expanded craters. (For interpretation of the references to colour in this figure legend, the reader is referred to the web version of this article.)

at CTX coverage for each crater, where available, to determine whether ice was present within the crater infilling material and/or within the ejecta layer(s) based on superposed expanded secondary craters. Fig. 10 shows the results of this survey. In order to maintain consistency with the present study, other indications of ice in the older primary craters, including concentric crater fill, were not accounted for here. Fig. 10 clearly shows that

thermocarstically-altered secondary craters are found on the ejecta of many preserved craters, including not only DLE craters but also SLE and MLE craters. However, since the expanded craters in the region of Arcadia Planitia are largely thought to be secondaries in origin and the overall distribution of secondary craters is fundamentally heterogeneous (with a radial orientation to the source primary crater), it is important to note that the lack of superposed expanded secondary craters is not necessarily diagnostic of a lack of subsurface ice. Furthermore, this metric is unable to identify features that contain pore-filling ice, although this type of ice is likely abundant, especially towards higher latitudes.

We also conduct a lower-resolution analysis of four additional DLE craters (labeled a–d in Fig. 10) with superposed expanded craters in the vicinity of the Arcadia Planitia study area. We measured the diameters of a sampling of these expanded craters using a single CTX image of each additional primary crater. These results are summarized in Fig. 11. In all cases, mean and median expanded crater diameters were higher in the inner ejecta, although only two of them (craters A and B, marked with asterisks in Fig. 11) had a difference that was statistically significant using the Mann-Whitney U-test ( $P < 0.05$ ). Due to the coarser mapping resolution used in this overview, far fewer secondary craters were used in this analysis compared to the more detailed study DLE crater. Nevertheless, these results suggest that other DLE craters have similar variations in excess ice content between ejecta layers.

## 5. Quantification of subsurface ice content

The volumes of all non-overlapping, expanded secondary craters were measured using the methods described in Viola et al. (2015), summarized here: a pre-impact surface was interpolated over the crater from the terrain immediately surrounding the edge of the crater using the Natural Neighbor technique in ArcGIS's 3D Analyst tools, and the DTM topography of the crater was extracted. Crater volumes were calculated by subtracting the topography of each crater from the pre-impact interpolation. We infer that the

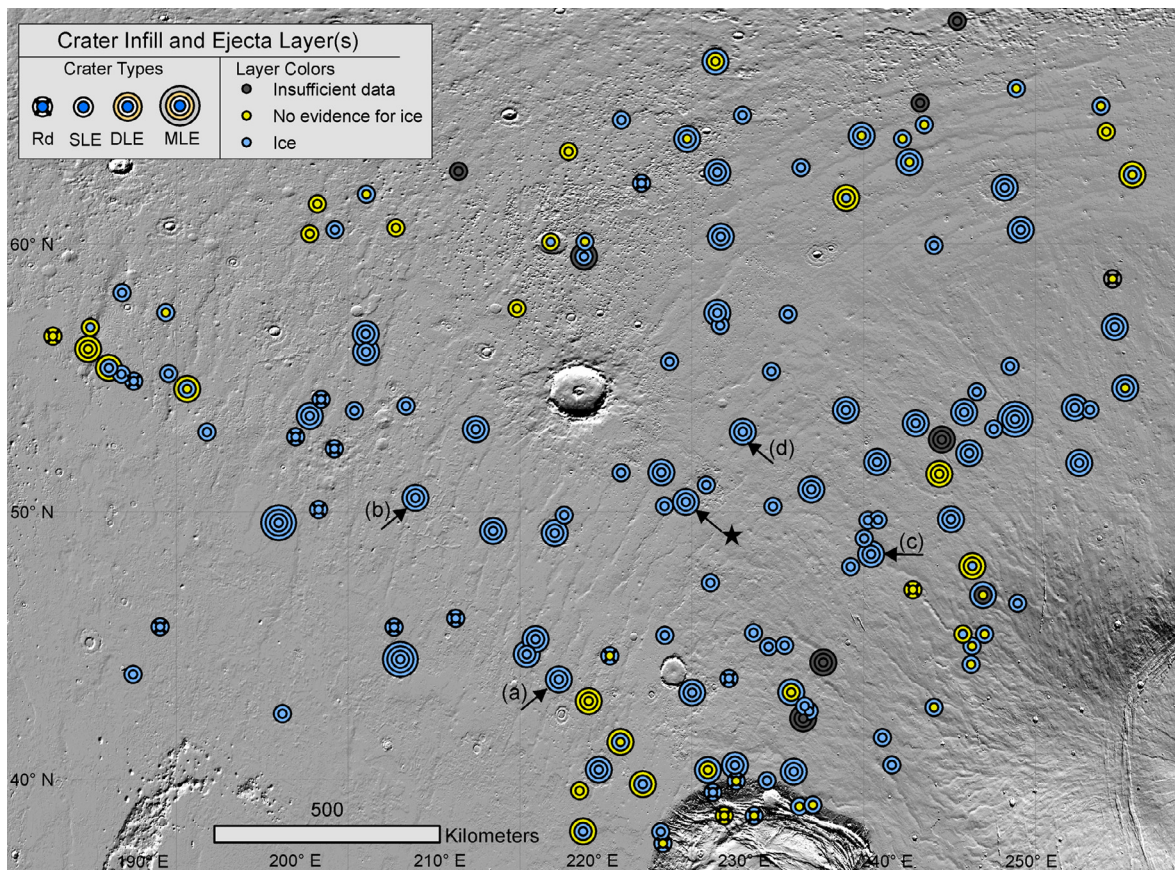


**Fig. 10.** This map shows the distribution of ice in the central bowl and ejecta layers well-preserved primary craters ( $D > 5$  km) in Arcadia Planitia. Each center point represents crater infilling material, and each subsequent ring represents an ejecta layer. Center points and ejecta layers are colored based on whether ice can be inferred by the presence of superposed expanded secondary craters, where light blue represents the presence of ice, yellow represents a lack of superposed expanded craters, and dark gray represents locations where there was insufficient CTX coverage to make a determination. The black arrow near the center of the map (labeled with a star) shows the location of the DLE crater used in this study, and the craters marked (a)–(d) correspond to the geographic locations of the additional craters analyzed in Fig. 11. (For interpretation of the references to colour in this figure legend, the reader is referred to the web version of this article.)

volume of expanded craters is an appropriate approximation of the volume of subsurface excess ice that was sublimated, as described previously.

A total of 6826 secondary craters within the three DTMs were non-overlapping, and 2453 of them were classified as expanded and could therefore be used in the crater volume analysis. It is important to note that non-overlapping craters do not fully represent the complete data set, since larger or more expanded craters are more likely to intersect with neighboring craters. Statistical tests have demonstrated this bias, showing that the non-overlapping subset is skewed towards smaller diameters compared to the complete dataset.

The use of current expanded volumes as a proxy for ice loss results in a conservative estimate due to two primary factors that would reduce the apparent amount of expansion: (1) ejecta tends to be more porous than the initial target material, and (2) eolian infill, which would contribute to shallowing the crater over time. It is also likely that some of the material initially ejected from the secondary craters was composed of excess ice, which would sublimate directly instead of collapsing into the crater during expansion. This would suggest that the current crater volume is the sum of the initial volume plus the volume of ice lost to sublimation during expansion. However, given the assumption that initial crater and rim volumes were approximately the same, the volumes would still reflect the total amount of ice sublimated even though not all of that volume was due to expansion-related sublimation.

### 5.1. Volumes of expanded craters

The median volume of non-overlapping expanded craters in all three regions was rather similar:  $76.4 \text{ m}^3/\text{km}^2$  on the inner ejecta,  $31.6 \text{ m}^3/\text{km}^2$  on the outer ejecta layer, and  $39.2 \text{ m}^3/\text{km}^2$  in the surrounding terrain. However, the mean values are skewed towards higher volumes:  $216 \text{ m}^3/\text{km}^2$  on the inner ejecta,  $65.5 \text{ m}^3/\text{km}^2$  on the outer ejecta, and  $65.8 \text{ m}^3/\text{km}^2$  in the surroundings. This suggests that all regions contain abundant small expanded craters, but also that more excess ice was generally lost from the inner ejecta secondary craters during the expansion process.

We find that the relationships between expanded crater volumes and diameters are roughly the same among the three regions of interest, as demonstrated by Fig. 12, where the expanded crater volume is roughly proportional to the diameter cubed. This suggests that the crater expansion mechanism has operated in a similar fashion regardless of location. We can therefore perform a polynomial regression on the data in Fig. 12, which results in the equation below (where  $V$  is the expanded crater volume in cubic meters and  $D$  is the expanded crater diameter in meters).

$$V = 0.0018D^{3.3319}$$

This equation allows us to estimate the volumes of the expanded craters that were overlapping in order to help mitigate the inherent biases of the volume measurement procedure, including extrapolations of the volumes of some of the largest craters in the data set. Accounting for all overlapping expanded craters shifts the

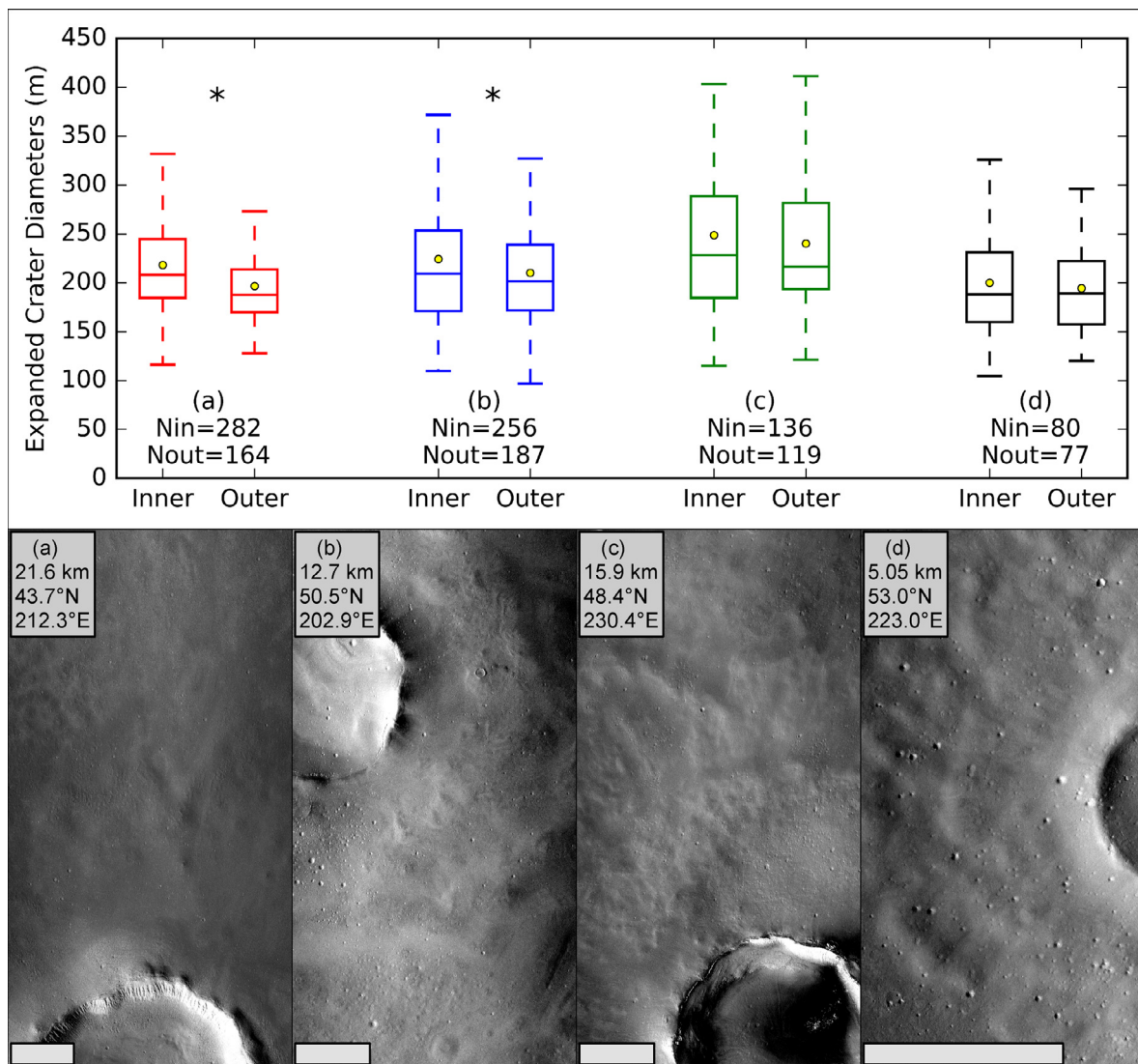


**Fig. 11.** Four other examples of DLE craters in the vicinity of Arcadia Planitia where a sampling of superposed expanded craters were measured using CTX data. (Top) Boxplot showing the variation in crater diameters on the inner and outer ejecta layer of each crater. Yellow points within boxplots represent mean values. In all cases, the mean expanded crater diameters are higher in the inner ejecta layer, although only craters A and B show a statistically significant difference between the ejecta layers. Scale bars in each image are 5 km. CTX images used are: (a) P03\_002316\_2234\_XN\_43N147W; (b) P21\_009344\_2299\_XI\_49N155W; (c) B18\_016767\_2288\_XI\_48N129W; and (d) G23\_027092\_2332\_XN\_53N136W. (For interpretation of the references to colour in this figure legend, the reader is referred to the web version of this article.)

median and mean crater volumes in each location to larger values due to the fact that larger craters are more likely to experience overlaps with neighboring craters. The adjusted median volume for craters in the inner ejecta layer, the outer ejecta layer, and the surrounding terrain is, respectively,  $116.7 \text{ m}^3/\text{km}^2$ ,  $41.7 \text{ m}^3/\text{km}^2$ , and  $44.5 \text{ m}^3/\text{km}^2$ , while the mean values for each location are  $589 \text{ m}^3/\text{km}^2$ ,  $84.6 \text{ m}^3/\text{km}^2$ , and  $68.7 \text{ m}^3/\text{km}^2$ .

#### 5.1.1. Inner ejecta layer

The inner ejecta layer accounts for a total mapped DTM area of  $67.9 \text{ km}^2$ . The expanded craters themselves cover 15% of the area of the inner ejecta layer that was mapped. The total volume of non-overlapping craters was  $7.39 \times 10^6 \text{ m}^3$ , and a total volume loss when accounting for overlapping craters is  $3.67 \times 10^7 \text{ m}^3$ . We can approximate the equivalent depth of ice lost from all expanded craters in this region from the total volume and the areal coverage of expanded craters. This calculation estimates that  $\sim 3.24 \text{ m}$  of ice was lost from the inner ejecta layer. This is an underestimate of the total thickness of excess ice in the region, as it assumes that the same depth of ice was lost from all expanded craters and, sim-

ilarly, that all points within each crater lost the same thickness of ice. In reality, we would expect a smaller thickness of ice to be lost from the smaller craters, and the deepest expanded craters (with depths that are greater than this 3.4-m thickness) must have lost much more ice. However, this approximation offers a minimum constraint on the amount of ice lost, and has implications on the amount of ice that is presently inflating the terrain immediately surrounding the expanded craters.

#### 5.1.2. Outer ejecta layer

The outer ejecta layer accounts for a total mapped DTM area of  $195.6 \text{ km}^2$ . The expanded craters themselves cover 10.6% of the section of the outer ejecta layer that was mapped. The total volume of non-overlapping craters was  $1.73 \times 10^7 \text{ m}^3$ , and a total volume loss when accounting for overlapping craters is  $3.77 \times 10^7 \text{ m}^3$ . This translates to an estimated minimum depth of 1.80 m of ice lost from the expanded craters in the outer ejecta layer and remaining in the un-cratered regions of the outer ejecta layer, although this is again most likely a significant underestimate of the actual amount of ice present.

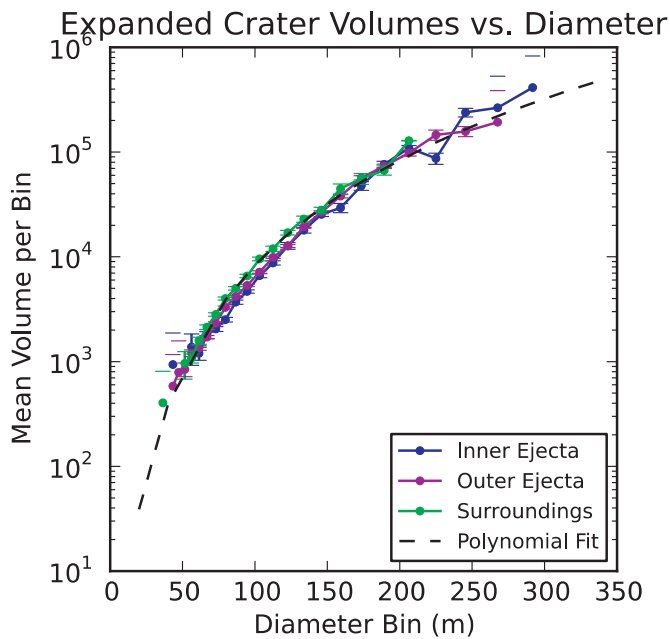


**Fig. 12.** The relationship between expanded crater volumes and diameters. Expanded craters in each location (inner ejecta, outer ejecta, and surroundings) all follow roughly similar trends, as shown by the polynomial regression.

### 5.1.3. Surrounding terrain

The surroundings account for a total mapped DTM area of 146.6 km<sup>2</sup>. The expanded craters themselves cover only 4.9% of the part of the surrounding terrain that was mapped. The total volume of non-overlapping craters was  $5.73 \times 10^6$  m<sup>3</sup>, and a total volume loss when accounting for overlapping craters is  $1.02 \times 10^7$  m<sup>3</sup>. This suggests that an estimated 1.45 m of ice was lost from the expanded craters in the surrounding terrain. When the hummocks that contain high concentrations of expanded craters are removed from the dataset, a similar calculation yields an estimated 1.42 m of ice lost throughout the plains region, which is only slightly lower than the estimate above.

### 5.2. Crater depths

Expanded crater depths may relate to more than just the initial penetration depth of the impact event; the deepest craters may, in fact, provide an estimate of the thickness of the ice into which they impacted. This is due to the fact that significant expansion requires that the ice is of a thickness that is at least roughly comparable to the crater depth (Viola et al., 2015) as opposed to penetrating through an ice layer that is only a small fraction of its depth, which would not experience sufficient material loss to produce the substantial diameter expansion that we observe. Expansion can also occur in ice layers much thicker than the crater depth (Dundas et al., 2015). Many of the smaller expanded craters likely only impact into the uppermost meters of the ice layer, but some of the largest might actually penetrate through the ice layer and into the underlying material. Evidence for this can be found in the depth-to-diameter ratios of the expanded craters, which increases with increasing diameter (Fig. 9). This suggests that there is proportionally less diameter expansion taking place relative to the crater's depth, which is the expected result for a case where the ice layer is thinner than the crater depth but still comprises a significant fraction of the crater's initial depth, although this could also be due to the smaller fractional growth required to produce a lag of a given thickness in a larger crater. Therefore, we posit that crater depth can be a useful metric for assessing ice con-

tent. While the median and mean crater depths from the non-overlapping craters in each region are low ( $\sim 1$ – $3$  m, Table 3), the many smaller craters likely only penetrate into the uppermost part of the excess ice layer. The largest expanded craters, however, are much deeper, and can provide an estimate of the thickness of the subsurface ice layer. Among the non-overlapping craters in each region of interest, the deepest were 17.9 m, 12.8 m, and 12.2 m in the inner ejecta, outer ejecta, and surrounding terrain, respectively (Table 3). However, the largest few expanded craters within the ejecta layers were overlapping, as well as the largest crater in the surrounding terrain. Therefore, we manually measured the depths of the two largest craters in each region based on the elevation of points that did not intersect with neighboring craters (Table 3). Here, we find that the deepest two overlapping expanded craters on the inner ejecta are 57 m and 27.1 m deep, compared to 21.7 m and 14.3 m in the outer ejecta and 14.8 m and 9.4 m (shallower than the largest non-overlapping crater) in the surrounding terrain. Measuring individual craters may be significantly affected by smaller-scale heterogeneities in ice thickness, so to obtain a more conservative estimate of the maximum ice thickness, we averaged the depths of the two deepest craters in each region: 42.1 m in the inner ejecta, 18 m in the outer ejecta, and 13.5 m in the surrounding terrain. The largest craters may have penetrated through the excess ice layer and been proportionally less affected by expansion, but it is also reasonable to expect that the initial (deeper) depths would provide a more valid metric rather than the present, modified depths that we can observe and describe here.

Craters that penetrate through a weak upper layer (such as ice) and a strong lower layer typically have terraced morphologies (e.g., Bramson et al., 2015). The crater expansion process may erase any terraces that were once present, but there is also a non-expanded, primary crater superposed on the inner ejecta layer with a depth of  $\sim 120$  m that does not have a terrace. This suggests that there was no significant strength contrast within the uppermost 120 m of the inner ejecta and offers a different constraint on ice thickness, comparable to the total ejecta thickness. This is more consistent with the estimates provided by the largest expanded craters. Therefore, the present maximum expanded crater depths only offer a rough order-of-magnitude constraint on the ice thickness, but nevertheless suggest that a significant quantity of ice remains in the subsurface today.

Expanded crater depths have further implications on the depth to the top of the subsurface ice. Since thermokarstic expansion requires the exposure or destabilization of excess ice, the shallowest craters that underwent expansion must have penetrated close to or into the upper part of the ice layer. Expanded craters with depths of  $< 0.5$  m can be found in all three regions of interest (inner ejecta, outer ejecta, and surrounding terrain), suggesting that the ice layer begins fairly close to the surface. It is worth noting that this depth to ice is significantly less than the ejecta thicknesses that Black and Stewart (2008) predict are necessary to armor ice from sublimation on long timescales, although ice may be more stable at this latitude. Therefore, it is plausible that the presently-accepted models may be insufficient to describe the observations here, where excess ice appears to be preserved at shallow depths on timescales that span multiple climate cycles. Updated modeling that accounts for the formation of lag deposits and deposition of pore-filling ice may help to resolve these inconsistencies. Preliminary results suggest that these processes increase the stability of excess ice, allowing it to persist for longer periods of time at shallower depths (Bramson et al., 2016).

### 5.3. Summary of observations

These results demonstrate that there were differences in the amount of ice present in each region at the time when the

**Table 3**  
Crater depths in each region of the DLE crater.

	Mean d	Median d	Largest d (non-overlapping)	Largest d (overlapping)	2nd largest d (overlapping)
Inner ejecta	2.65 m	1.94 m	17.9 m	57.0 m	27.1 m
Outer ejecta	2.16 m	1.57 m	12.8 m	21.7 m	14.3 m
Surroundings	1.49 m	1.10 m	12.2 m	14.8 m	9.4 m

superposed secondary craters formed. Since the expanded craters are present today, significant dissection of the excess ice layer that they impacted into could not have taken place. Therefore, it is likely that these differences persist to this day, where measurements of expanded crater volumes provide a lower limit on the amount of ice remaining, suggesting that a thicker layer of excess ice remains in the near-surface of the inner ejecta layer (at least 3.4 m) and that the surrounding terrain contains a thinner ice layer, at least 1.4 m in thickness.

An alternative method for estimating ice thickness is based on crater depths. It has been hypothesized that expanded crater depths may be related to the depth/thickness of excess ice and that they may require an excess ice layer at least comparable to, if not deeper than, the depth of the crater. Therefore, the maximum depths of expanded craters could be connected to the amount of ice that was present when the craters formed, although these are possible overestimates since the largest craters may penetrate through the subsurface ice layer. In all three regions of interest, manual measurements of the largest expanded craters suggest that this DLE crater may contain ice thicknesses much greater than the lower limits described above, possibly comparable to the total ejecta thickness.

Smaller-scale heterogeneities in the ice content of each region may also play a role in the total amount of ice present within the DLE crater, particularly in the case of the individual craters measured. Nevertheless, these two methods offer both lower and possible upper limits of the ice content within the DLE crater and the surrounding terrain.

#### 5.4. Extrapolations of present ice content in ejecta

The estimates of ice thickness in this section suggest that a thickness of at least  $\sim 3.4$  m (and potentially 42.1 m or more) of excess ice must remain throughout the un-cratered parts of the inner ejecta layer. The inner ejecta covers a total spatial area of 900 km<sup>2</sup> and assuming the same rate of superposed cratering as was measured in the DTMs, we estimate that a total of 2.8 km<sup>3</sup> (and possibly  $\geq 35$  km<sup>3</sup>) of excess ice remains preserved in the inner ejecta. The outer ejecta covers a total area of 2400 km<sup>2</sup> and has an ice thickness of at least 1.8 m (up to 18 m). This translates to a total of 3.9–39 km<sup>3</sup> still preserved in the un-cratered parts of the outer ejecta. Therefore, the entire extent of the ejecta deposit may contain as much as 74 km<sup>3</sup> of ice, or more if the largest expanded craters did not penetrate the ice-rich layer.

## 6. Discussion

Since expanded secondary craters are found throughout the entire region in which this DLE crater is found, excess ice must be widespread. However, since the number of expanded craters and the degree of expansion varies among the inner ejecta layer, the outer ejecta layer, and the surrounding terrain, we posit that the amount of excess ice in each region (depth, thickness, and/or regolith content) similarly varies. It is possible that the initial size frequency distribution of secondary craters may have varied along the length of the secondary crater ray. However, the stark differences in expanded crater diameters that correlate with the bounds

of each ejecta layer are unlikely to be a coincidence. This suggests that at least part of the observed difference in secondary crater expansion is the result of differences in the material properties of the surface and shallow subsurface of each layer of ejecta and the surrounding terrain. Since crater expansion requires the presence of subsurface excess ice, it is therefore likely that the degree of crater expansion should be correlated to the depth and volume of ice present in the near subsurface. The results shown in Figs. 5 and 7 indicate that there are more expanded craters overlying the inner ejecta layer, and that there are the fewest expanded craters in the surrounding terrain. This suggests that the most excess ice was present in the inner ejecta layer at the time when the superposed secondary craters formed. It is also likely that there is more ice present there today (as much as  $\geq 35$  km<sup>3</sup> in the inner layer, and  $\geq 75$  km<sup>3</sup> for the entire ejecta deposit), since there is no apparent terrain dissection in the region that would have resulted in the loss of the superposed expanded craters.

It is clear that the study DLE crater has been modified after its formation by glacial/periglacial, impact, and erosional processes, demonstrated in part by the presence of expanded craters overlying the ejecta layers and within the crater itself. Infilling material is evident within the crater bowl, with concentric lineations most apparent in the sections of the bowl that are not heavily modified by superposed expanded craters (Fig. 3c). This concentric crater fill (CCF) has been observed throughout the mid-latitudes on Mars, and while a variety of hypotheses have been proposed, including a purely aeolian mechanism (Zimbelman et al., 1989), CCF is most likely the result of glacial processes influencing atmospherically deposited ice. Levy et al. (2010) relate CCF to other martian glacial morphologies, including lineated valley fill (LVF) and lobate debris aprons (LDA), and extend the hypothesis of debris-covered glaciers to explain all three morphologies (LVF, LDA, and CCF). Dickson et al. (2010) propose that CCF is composed of remnant ice from past glaciation events, where kilometer-scale ice sheets were deposited during climate shifts and preferentially remain within craters as the climate shifts back. It has also been suggested that the accumulation of CCF requires multiple ice deposition events, where only ice on the steep crater slopes can flow into the crater and is protected from sublimation by debris from the crater wall, and the entire crater is filled over successive glaciation events (Fastook and Head, 2014).

Since a new ice-exposing impact (Site 16 in Dundas et al., 2014) has been observed within the infilling material in this DLE crater, it is clear in this case that ice is still present to this day. Furthermore, the DLE crater fill contains expanded secondary craters (Fig. 3d) that were likely sourced by the same impact event that produced the secondaries on the ejecta, indicating that the CCF-forming event must have pre-dated the formation of the superposed secondary craters. It is possible that there are multiple layers of excess ice, and that the thermokarstically-altered secondary craters and the recent ice-exposing impact sample two different regions of excess ice. Nevertheless, this adds an extra layer of complexity to the history of the study DLE crater, as we will describe.

We also note the presence of several small hills in the terrain surrounding the DLE crater. Small hummocks with fine-grained surfaces were also identified near several DLE craters in Acidalia Planitia by Komatsu et al. (2007). Several hypotheses were pro-

posed to explain these features based on their mound-like morphology, including pingos (ice-cored mounds) and mud volcanoes. Pingos, which are commonly found in terrestrial periglacial regions and form from pressurized groundwater that freezes to produce an ice core, have been hypothesized on Mars, particularly in the northern hemisphere (Burr et al., 2009) and notably in Utopia Planitia (Osinski and Soare, 2007; Soare et al., 2005; de Pablo and Komatsu, 2008; Dundas et al., 2008). Fractured mounds consistent with pingos have further been identified in the mid-latitudes of both hemispheres (Dundas and McEwen, 2010). However, the mounds surrounding this DLE crater do not possess fractures similar to those that develop on terrestrial pingos, and much previous work concedes that it is unclear whether the high water volumes required to form terrestrial-style pingos were present on Mars (e.g., Dundas and McEwen, 2010). Mud volcanoes would also suggest high volatile content, but this hypothesis would require high enough subsurface temperatures for liquid water that may be unrealistic for Mars unless the activity were shock-induced and related to the impact event itself (Komatsu et al., 2007). These would both suggest high volatile content consistent with observations of both Acidalia and Arcadia Planitiae and by the presence of fluidized ejecta deposits. However, the simplest explanation for these hills is that they are simply remnants of a past icy layer that was once more extensive. This would be consistent with the glacial substrate model (Weiss and Head, 2013), which posits that DLE craters form from impacts into surface ice that is subsequently lost on broad scales.

There are several potential sources of ice that can account for the volatile distribution seen in the different ejecta layers. First, it is possible that the ice present in the ejecta has been there since the original impact and was preserved differently within the ejecta layers. However, this would not explain the presence of concentric crater fill, since the deposition of glacial infill must post-date the DLE-forming impact and predate the formation of the expanded secondaries. This would suggest additional ice deposition took place after the crater formed. Second, if the excess ice was formed from ice lenses in the subsurface, then it is possible that the original material properties of the crater ejecta differed such that the inner ejecta layer was more conducive to ice lens development and growth. This also would not account for concentric crater fill. However, if the CCF-forming event was more localized (for example, ice was preferentially deposited only on the shadowed crater wall and slowly flowed into the rest of the crater) or if it resulted from the deposition and loss of ice on the ejecta that did not alter the subsurface deposits, the first two hypotheses for ice deposition can still be valid. Third, it is possible that all of the ice was deposited after crater formation in the form of snowfall or large-scale glaciation. This may be consistent with the observation of ice-rich concentric crater fill within the crater bowl, but such large-scale ice deposition means that the entire crater would have been buried in ice at some point in its past. In this case, it is unclear why more ice would have been deposited and/or preserved in the inner ejecta as compared to the outer ejecta and surrounding terrain, although it is conceivable that material properties could have contributed to this difference.

An intriguing alternative source of ice may be related to hydrothermal activity. Some terrestrial craters contain mineralogical evidence for impact-induced hydrothermal activity (e.g. Osinski et al., 2001; Zurcher and Kring, 2004), and has also been proposed for Mars (Abramov and Kring, 2005). However, it is thought that most of this activity may be concentrated within the central peak or peak-ring structures (Abramov and Kring, 2005), consistent with observations of Hesperian-aged Toro crater (Marzo et al., 2010). Hydrated silicates have been observed within crater ejecta, and although several studies attribute this to impact-excavated material, it has been argued that terrestrial (and possibly martian) craters

contain evidence for hydrothermal alteration (Osinski et al., 2013). If hydrothermal activity could concentrate water/ice closer to the crater, then the present distribution of these materials in the study DLE crater may be unrelated to the ejecta emplacement mechanism. However, there is no clear mechanism for hydrothermal activity to produce excess ice within the ejecta.

An ejecta-armoring mechanism has been suggested for low-aspect-ratio layered ejecta (LARLE) craters, which have both normal layered ejecta and a more extensive, thin outer deposit. Barlow et al. (2014) propose that water migration within the LARLE deposit transports salts to the surface, which forms a duricrust that protects the deposit from rapid removal. However, we do not observe a LARLE deposit around the primary DLE crater, and it is unclear whether this mechanism can operate for non-LARLE craters.

The expanded craters found in the surrounding terrain indicate that there was excess ice throughout the region at the time of secondary crater emplacement. It is also conceivable that, in the case of the surrounding terrain, the subsurface ice may be older than the DLE crater, suggesting the presence of volatiles at the time that the DLE crater formed.

While this analysis only considers a single double-layer ejecta crater based on the fortuitous presence of extensive thermokarstic alteration, there are broader implications for the formation of DLE craters in general that we will investigate. This is particularly true in light of the fact that many other DLE craters show similar evidence of being ice-rich today (Fig. 10), and that some appear to have similar variations in the ice content between the ejecta layers (Fig. 11). Table 4 briefly summarizes our results, compared to the expectations of the different DLE-formation hypotheses. Each possibility is described in further detail below.

### 6.1. Ice preserved from impact

The first section of Table 4 summarizes the case where the ice was preserved from the time of impact and DLE-crater formation, which is strongly dependent on the formation mechanism. The glacial substrate model implies that ice from the time of impact is preserved beneath the crater ejecta, and it is worth noting that the estimated ice thicknesses for the ejecta layers discussed in Section 5.2 are roughly comparable to the estimated thickness of surficial deposits predicted for DLE craters in Weiss and Head (2014), consistent with that model. However, it is possible that the preserved ice would be at a depth that is greater than the depth to which the superposed craters penetrated. Modeling results suggest that thicker ejecta is more efficient at protecting subsurface ice from sublimation, where ejecta thicknesses of >10 m were able to preserve ice for tens of millions of years (Black and Stewart, 2008). Applied to the glacial substrate model, it would be expected that the thicker, inner ejecta layer of DLE craters is more likely to preserve abundant ice, consistent with our qualitative observations. However, while the timescales presented by Black and Stewart (2008) are consistent with the estimated age of the superposed expanded craters, it requires overlying ejecta deposits that are thicker than the expected depth to the ice layer proposed in Section 5.2. This issue may be resolved by more sophisticated modeling (Bramson et al., 2016), which suggests that the deposition of pore-filling ice within the regolith above a mid-latitude excess ice layer can help to protect the excess ice from sublimation on longer timescales.

In the case of subsurface ice-rich layers (Senft and Stewart, 2008), we may similarly expect more ice in the inner ejecta layer due to the fact that thicker inner ejecta is clearly produced. However, it is again possible that this ice would also need to be buried under thicker ejecta deposits in order to remain preserved.

If the preserved ice is a relic of volatiles involved in DLE crater formation, our findings would also be fundamentally incongruous

**Table 4**  
Summary of DLE formation hypotheses.

Formation hypothesis	Ice preserved from impact		Ice lenses (particle-size dependent)	
	Inner Ejecta	Outer Ejecta	Inner Ejecta	Outer Ejecta
<b>Results (this study)</b>				
Atmospheric effects (Schultz & Gault 1979)				
Presence of volatiles (Mouginis-Mark, 1981)				
Base surge (Boyce & Mouginis-Mark 2006)	?			
Dry granular flow (Wada & Barnouin-Jha, 2006)			?	?
Impact melt (Osinski 2006)		?	?	?
Combination effects (Komatsu et al. 2007)	?	?		
Subsurface icy layers (Senft and Stewart, 2008)	*			
Ballistic sedimentation in layered targets (Oberbeck, 2009)				
Glacial substrate model (Weiss & Head, 2013)	*			
Landslide ice/regolith (Wulf & Kenkmann 2015)				

More Ice/water	Less Ice/water
No Ice/water	Equal Ice/water
?	Uncertain
*	May require thicker ejecta deposit

with the model proposed by [Wulf and Kenkmann \(2015\)](#), where the outer ejecta is expected to be wetter than the inner ejecta.

The presence of volatiles as proposed by [Mouginis-Mark \(1981\)](#) suggests that the inner ejecta layer would have formed from dry materials and the outer ejecta formed from wet materials, which is also inconsistent with our observations. The updated base surge hypothesis suggests that the inner ejecta forms in a manner that is similar to SLE craters. Since observations show that SLE craters are widely distributed on the martian surface ([Barlow, 2015](#)), this does not necessarily require high concentrations of water for formation. Ballistic sedimentation in ice/water-rich layered

deposits ([Oberbeck, 2009](#)) also argues that both SLE deposits and the inner ejecta layer of DLE craters is emplaced ballistically akin to lunar craters, and is thus expected to be dry.

The impact melt hypothesis of [Osinski \(2006\)](#) argues that the outer ejecta layer is emplaced ballistically, and is not necessarily water-rich, while the inner ejecta layer forms as a ground-hugging flow comprised of impact melt and water derived from both the target rock and subsurface ice. This may be consistent with our observations of present-day ice distributions if the ice is a remnant of DLE crater formation.

The dry granular flow mechanism proposed by [Wada and Barnouin-Jha \(2006\)](#) does not require the presence of volatiles, and therefore would not necessarily suggest preservation of water/ice from the time of impact. The atmospheric effect hypothesis first proposed by [Schultz and Gault \(1979\)](#) also does not require the presence of water at the time of DLE crater formation. It is unclear how the presence of water might affect these two models. However, the combination volatile/atmospheric mechanism proposed by [Komatsu et al. \(2007\)](#) suggests that water is involved in the formation of both ejecta layers: the inner ejecta forms as a water-rich flow, and the outer ejecta forms ballistically from water-rich materials that interact with the atmosphere. Since it is unclear which layer would be expected to form from more water-rich materials, this mechanism cannot be ruled out.

It should be noted that more than one process may have operated. For instance, base surges or impact-melt processes could occur in concert with a glacial substrate.

## 6.2. Ice lenses

The second section of [Table 4](#) summarizes the case where the excess ice actually formed after the DLE crater, in the form of subsurface ice lenses. [Sizemore et al., \(2015\)](#) found that regolith with abundant perchlorate salts or smaller particle sizes tended to allow for more ice lens growth. Applied to this scenario, we would posit that, if ice lenses sourced the excess ice, then the inner ejecta layer would have been composed of more salt-rich or finer-grained material than the outer ejecta layer. However, it is difficult to justify different salt concentrations associated with the ejecta layers, and the observations of particle size variations within the ejecta of a few DLE craters generally indicate that the outer ejecta layer is composed of finer-grained particles compared to the inner ejecta. Furthermore, many of the formation mechanisms agree with this particle size distribution. For example, in the base surge hypothesis, the outer ejecta layer is formed from the collapse of lofted fine-grained materials ([Boyce and Mouginis-Mark, 2006](#)). The outer ejecta layer is also expected to be largely comprised of finer-grained materials in the combination mechanism ([Komatsu et al., 2007](#)), the atmospheric effects hypothesis ([Schultz and Gault, 1979](#)), and ballistic sedimentation in layered targets ([Oberbeck, 2009](#)). The models that invoke landslide events to form the inner ejecta ([Weiss and Head, 2013](#); [Wulf and Kenkmann, 2015](#)) would suggest coarser-grained materials in the landslide deposits, particularly because larger ejecta fragments tend to be deposited closer to the crater while smaller particles are deposited further away ([Horz et al., 1983](#); [Melosh, 1989](#)). [Senft and Stewart \(2008\)](#) suggest that the presence of subsurface icy layers modifies the trajectories of ejecta emplacement, where most of the material is deposited close to the crater rim, but similarly, larger ejecta fragments would still likely be deposited nearest the crater. These are all inconsistent with the smaller particle sizes required for the inner ejecta to be more conducive to ice lens growth. Additionally, it is unlikely that ice lenses would produce excess ice thicknesses approaching the overall ejecta thickness, as suggested by the non-terraced primary crater discussed above. Therefore, we infer that ice lenses are likely not the primary mode of ice deposition within the shallow

subsurface of this DLE crater, unless particle sizes are controlled by post-impact processes. However, they may have influenced the near-surface ice distribution

It is conceivable that different patterns of ice lens growth would be possible if post-impact processes altered the initial particle sizes present at the time of formation. For example, in volcanic terrains, observations have found that dust and fine-grained particles tend to be preferentially trapped in regions that are rougher at small scales (Malin et al., 1983; Zimbelman, 1990), perhaps analogous to the rougher inner ejecta here. In this case, we might expect that the inner ejecta would have captured more dust, making it more conducive to ice lens growth over time. However, while this may help account for the current particle size homogeneity observed today (Fig. 4), it is unclear whether sufficient dust could have been trapped in the inner ejecta to be able to account for the differences in ice content between the two ejecta layers.

### 6.3. Subsequent snowfall/post-impact deposition

Cycles of obliquity-driven climate change on Mars have led to fluctuations in the regions where surface and subsurface ice is stable (Mellon and Jakosky, 1995; Laskar et al., 2004; Chamberlain and Boynton, 2007). This leads to net transport of ice from the poles to the mid-latitudes during periods of high obliquity (Jakosky and Carr, 1985; Head et al., 2003) or from the equator during moderate to low obliquity periods (Madeleine et al., 2009; Levrard et al., 2004). It would therefore seem reasonable that some deposition has taken place in this study area since the formation of the DLE crater. In fact, it is clear from the presence of expanded secondaries within the concentric crater fill of the DLE crater that some ice deposition took place after the formation of the DLE crater but before the emplacement of the superposed secondary craters. However, this does not necessarily mean that there was widespread ice deposited over the entire region; it is alternatively possible that, during CCF formation, ice was preferentially deposited on cooler slopes on the crater walls and then flowed downslope to fill the crater bowl. If ice was widely distributed over the entire area during a period of high obliquity and effectively removed everywhere except within the crater bowl during a period of lower obliquity (Fastook and Head, 2014), then either the surficial deposits did not affect the presence of excess ice preserved within the ejecta, or the ice in the ejecta post-dates the CCF-forming event, perhaps in the form of ice lenses. This ultimately suggests that ice was deposited in different regions of the crater by multiple mechanisms over time, further complicating the history of this crater's formation and modification.

Factors that could affect ice deposition on the crater ejecta include variations in surface roughness, porosity, grain size, ejecta thickness, or other physical characteristics that can lead to more ice becoming trapped in some units as compared to others. However, it is unclear how small-scale textures and physical properties could affect the deposition of ice such that it would account for the differing amounts of ice that we see in the two ejecta layers today. It is similarly unclear how the two ejecta layers could have preferentially preserved different amounts of ice, assuming uniform deposition, particularly when the estimated ice thicknesses are enough to totally blanket the pre-existing substrate. As previously mentioned, dust retention on lava flows does vary with surface roughness, but this process relies on wind-transported material deposited in rougher regions that is trapped from future aeolian removal, and ice/snow deposition may not follow the same trend. Another possibility is that variations in thermal properties may have contributed to differential preservation between the ejecta layers. However, little work has been done to broadly characterize

the temperatures and thermal inertias of fresh, un-modified DLE craters.

Post-impact ice deposition may be most consistent with the observations based on the clear evidence for ice deposited within the crater. However, disentangling all the uncertainties of differential deposition or preservation between the ejecta layers is complex, and we leave this task to future study.

### 6.4. Summary of DLE crater formation mechanisms

It is possible that different modes of ice deposition may have contributed to the distribution observed today. For example, the crater fill is possibly unrelated to the ice preserved in the ejecta, due to a later ice deposition event that did not necessarily affect the ice preserved in the ejecta layers. However, after reviewing the expectations of the different formation mechanisms in the context of several types of ice deposition events, we find that none of the existing models seem to completely fit our observations of the volatile content within the ejecta layers, although some remain plausible. Therefore, it may be necessary to devise a new or modified model for DLE crater formation.

## 7. Conclusions

We observed expanded secondary craters superposing a double-layer ejecta crater in the vicinity of Arcadia Planitia. The crater expansion process, as described previously (Viola et al., 2015; Dundas et al., 2015), requires the presence of near-surface excess ice in order to take place. Furthermore, the long-term preservation of expanded craters such that we observe them today requires the persistence of excess ice from the time that expansion occurred. We consider the degree of superposed secondary crater expansion, as measured from crater diameters and volumes, to be a metric for the abundance of near-surface excess ice at the time that the expanded craters formed and which has persisted to the present day. Our measurements reveal that the degree of expansion is greater on the inner ejecta as compared to the outer ejecta, which suggests that the inner ejecta layer contained a higher abundance of excess ice at the time when the superposed secondary craters formed. However, it is challenging to discern when and why this difference originated. Some ice in the ejecta may have predated the DLE-crater forming event, while ice in the crater fill must post-date the event, and both must have occurred. The superposed secondary craters are on the order of tens of millions of years old, suggesting that the ice in the ejecta layers has persisted for at least that long, but we cannot determine the age of the DLE crater itself due to the significant secondary crater contamination.

Several mechanisms may have contributed to the deposition or development of excess ice. The mechanisms that we specifically consider are water or ice preserved from the time of impact, the initiation and growth of ice lenses, and the preferential deposition or preservation of ice during post-impact glacial activity. If the ice is relict from the time that the DLE crater formed, then the impact melt hypothesis (Osinski, 2006) is potentially consistent with our observations of this DLE crater. However, our observations are inconsistent with ice lenses as the sole method of excess ice formation due to the fact that finer grained materials are more conducive to ice lens growth (Sizemore et al., 2015) and the outer ejecta tends to be comprised of smaller particle sizes than the inner ejecta. Post-impact glacial activity clearly occurred based on the presence of glacial infill within the crater bowl, although it is difficult to assess the extent and duration of such activity and whether it affected the ejecta layers in such a way that it would lead to variations in ice content between the two ejecta layers.

The broader trend, where layered ejecta deposits tend to be ice-rich based on the presence of superposed expanded secondary

craters in Arcadia Planitia, may suggest that the ejecta has armored subsurface ice, protecting it from atmospheric losses. Tentatively, this may be most consistent with the glacial substrate model, which proposes that DLE craters form from impacts into surface ice deposits. However, the observed variation in ice content between the ejecta layers remains incompletely explained for this DLE formation mechanism, and could provide insights into the detailed dynamics of the ejecta.

## Acknowledgments

We would like to thank Nicholas Gizzi for the production of digital terrain models (DTMs) and Sarah Sutton for training/assistance on DTM production. Helpful reviews from Nadine Barlow and David Weiss greatly enhanced this work. Funding was provided through the High Resolution Imaging Science Experiment (HiRISE). All images and DTM products used in this study are available through the PDS (<http://img.pds.nasa.gov>).

## References

- Abramov, O., Kring, D.A., 2005. Impact-induced hydrothermal activity on early mars. *J. Geophys. Res.* 110, E12S09.
- Artemieva, N.A., Wünnemann, K., Krien, F., Reimold, W.U., Stoffer, D., 2013. Ries crater and suevite revisited—Observations and modeling. Part II: modeling. *Meteorit. Planet. Sci.* 48, 590–627.
- Bandfield, J.L., Feldman, W.C., 2011. Martian high latitude permafrost depth and surface cover thermal inertia distributions. *J. Geophys. Res.* 113, E08001.
- Baratoux, D., Mangold, N., Pinet, P., Costard, F., 2005. Thermal properties of lobate ejecta in syrtis Major, Mars: implications for the mechanisms of formation. *J. Geophys. Res.* 110, E04011.
- Barlow, N.G., 1994. Sinuosity of martian rampart ejecta deposits. *J. Geophys. Res.* 99, 10927–10935.
- Barlow, N.G., 2005. A review of martian impact crater ejecta structures and their implications for target properties. In: Kenkmann, T., Horz, F., Deutsch, A. (Eds.), *Large meteorite impacts III: Geological Society of America Special Paper 384*, pp. 433–442.
- Barlow, N.G., 2015. Characteristics of impact craters in the northern hemisphere of mars. In: Osinski, G.R., Kring, D.A. (Eds.), *Large Meteorite Impacts and Planetary Evolution V: Geological Society of America Special Paper 518*.
- Barlow, N.G., Bradley, T.L., 1990. Martian impact craters: correlations of ejecta and interior morphologies with diameter, latitude, and terrain. *Icarus* 87, 156–179.
- Barlow, N.G., Koroshetz, J., Dohm, J.M., 2001. Variations in the onset diameter for martian layered ejecta morphologies and their implications for subsurface volatile reservoirs. *Geophys. Res. Lett.* 28, 3095–3098.
- Barlow, N.G., Perez, C.B., 2003. Martian impact crater ejecta morphologies as indicators of the distribution of subsurface volatiles. *J. Geophys. Res.* 108, 5085.
- Barlow, N.G., Boyce, J.M., Cornwall, C., 2014. Martian low-aspect ratio layered ejecta (LARLE) craters: distribution, characteristics, and relationship to pedestal craters. *Icarus* 239, 186–200.
- Barnouin-Jha, O.S., Schultz, P.H., Lever, J.H., 1999a. Investigating the interactions between an atmosphere and an ejecta curtain: 1. wind tunnel tests. *J. Geophys. Res.* 104, 27105–27115.
- Barnouin-Jha, O.S., Schultz, P.H., Lever, J.H., 1999b. Investigating the interactions between an atmosphere and an ejecta curtain: 2. Numerical experiments. *J. Geophys. Res.* 104, 27117–27131.
- Black, B.A., Stewart, S.T., 2008. Excess ejecta craters record episodic ice-rich layers at middle latitudes on mars. *J. Geophys. Res.* 113, E02015.
- Boyce, J.M., Mouginiis-Mark, P.J., 2006. Martian craters viewed by the thermal emission imaging system instrument: Double-layered ejecta craters. *J. Geophys. Res.* 111, E10005.
- Boyce, J., Barlow, N., Mouginiis-Mark, P., Stewart, S., 2010. Rampart craters on Ganymede: their implications for fluidized ejecta emplacement. *Meteorit. Planet. Sci.* 45, 638–661.
- Boynton, W.V., Feldman, W.C., Squyres, S.W., Prettyman, T.H., Bruckner, J., Evans, L.G., et al., 2002. Distribution of hydrogen in the near surface of Mars: evidence for subsurface ice deposits. *Science* 297, 81–85.
- Bramson, A.M., Byrne, S., Putzig, N.E., Sutton, S., Plaut, J.J., Brothers, T.C., et al., 2015. Widespread excess ice in arcadia planitia, mars. *Geophys. Res. Lett.* 42, 6566–6574.
- Bramson, A.M., Byrne, S., Bapst, J.N., 2016. Preservation of excess ice in the northern mid-latitudes of mars. Sixth Mars Polar Science Conference Abstract #6074.
- Burr, D.M., Tanaka, K.L., Yoshikawa, K., 2009. Pingos on earth and mars. *Planet. Space Sci.* 57, 541–555.
- Byrne, S., Dundas, C.M., Kennedy, M.R., Mellon, M.T., McEwen, A.S., Cull, S.C., et al., 2009. Distribution of mid-latitude groundice on mars from new impact craters. *Science* 325, 1674–1676.
- Carr, M.H., Crumpler, L.S., Cutts, J.A., Greeley, R., Guest, J.E., Masursky, H., 1977. Martian impact craters and emplacement of ejecta by surface flow. *J. Geophys. Res.* 82, 4055–4065.
- Chamberlain, M.A., Boynton, W.V., 2007. Response of martian ground ice to orbit-induced climate change. *J. Geophys. Res.* 112, E06009.
- Christensen, P.R., Bandfield, J., Bell, J.F., Gorelick, N., Hamilton, V.E., Ivanov, A., et al., 2003. Morphology and composition of the surface of Mars: marsodyssey THEMIS results. *Science* 300, 2056–2061.
- de Pablo, M.A., Komatsu, G., 2008. Possible pingo fields in the utopia Basin, Mars: geological and climatic implications. *Icarus* 199, 49–74.
- Dickson, J.L., Head, J.W., Marchant, D.R., 2008. Late amazonian glaciation at the dichotomy boundary on Mars: evidence for glacial thickness maxima and multiple glacial phases. *Geology* 36, 411–414.
- Dickson, J.L., Head, J.W., Marchant, D.R., 2010. Kilometer-thick ice accumulation and glaciation in the northern mid-latitudes of Mars: evidence for crater-filling events in the lateamazonian at the phlegramontes. *Earth Planet. Sci. Lett.* 294, 332–342.
- Dundas, C.M., McEwen, A.S., 2010. An assessment of evidence for pingos on mars using HiRISE. *Icarus* 205, 244–258.
- Dundas, C.M., Mellon, M.T., McEwen, A.S., Lefort, A., Keszthelyi, L.P., Thomas, N., 2008. HiRISE observations of fractured mounds: possible martian pingos. *Geophys. Res. Lett.* 35, L04201.
- Dundas, C.M., Byrne, S., McEwen, A.S., Mellon, M.T., Kennedy, M.R., Daubar, I.J., et al., 2014. HiRISE observations of new impact craters exposing martian ground ice. *J. Geophys. Res.* 119, 109–127.
- Dundas, C.M., Byrne, S., McEwen, A.S., 2015. Modeling the development of martian sublimation thermokarst landforms. *Icarus* 262, 154–169.
- Fastook, J.L., Head, J.W., 2014. Amazonian mid- to high-latitude glaciation on Mars: supply-limited ice sources, ice accumulation patterns, and concentric crater fill glacial flow and ice sequestration. *Planet. Space Sci.* 91, 60–76.
- Feldman, W.C., Prettyman, T.H., Maurice, S., Plaut, J.J., Bish, D.L., Vaniman, D.T., et al., 2004. Global distribution of near-surface hydrogen on mars. *J. Geophys. Res.* 109, E09006.
- Fisher, D.A., 2005. A process to make massive ice in the martian regolith using long-term diffusion and thermal cracking. *Icarus* 179, 387–397.
- Garvin, J.B., Frawley, J.J., 1998. Geometric properties of martian impact craters: preliminary results from the mars orbiter laser altimeter. *Geophys. Res. Lett.* 25, 4405–4408.
- Head, J.W., Mustard, J.F., Kreslavsky, M.A., Milliken, R.E., Marchant, D.R., 2003. Recent ice ages on mars. *Nature* 426, 797–802.
- Holt, J.W., Safaeinili, A., Plaut, J.J., Young, D.A., Head, J.W., Phillips, R.J., 2008. Radar sounding evidence for ice within lobate debris aprons near hellas Basin, mid-southern latitudes of mars. In: 39th Lunar and Planetary Science Conference, p. 2441.
- Horz, F., Ostertag, R., Rainey, D.A., 1983. Bunte breccia of the Rles: continuous deposits of large impact craters. *Rev. Geophys. Space Phys.* 21, 1667–1725.
- Jakosky, B.M., Carr, M.H., 1985. Possible precipitation of ice at low latitudes of mars during periods of high obliquity. *Nature* 315, 559–561.
- Jones, E., Osinski, G.R., 2015. Using martian single and double layered ejecta craters to probe subsurface stratigraphy. *Icarus* 247, 260–278.
- Jones, E., Caprarello, G., Osinski, G.R., 2016. Insights into complex latered ejecta emplacement and subsurface stratigraphy in chryse Planitia, Mars, through analysis of THEMIS brightness temperature data. *J. Geophys. Res.* 121, 986–1015.
- Kirk, R.L., Howington-Kraus, E., Roseik, M.R., Anderson, J.A., Archinal, B.A., Becker, K.J., et al., 2008. Ultrahigh resolution topographic mapping of mars with MRO HiRISE stereo images: meter-scale slopes of candidate phoenix landing sites. *J. Geophys. Res.* 113, E00A24.
- Komatsu, G., Ori, G.G., Lorenzo, D., Rossi, P., A., Neukum, G., 2007. Combinations of processes responsible for martian impact crater “layered ejecta structures” emplacement. *J. Geophys. Res.* 112, E06005.
- Laskar, J., Correia, A.C., Gastineau, M., Joutel, F., Levrard, B., Robutel, P., 2004. Long term evolution and chaotic diffusion of the insolation quantities of mars. *Icarus* 170, 343–364.
- Levrard, B., Forget, F., Montmessin, F., Laskar, J., 2004. Recent ice-rich deposits formed at high latitudes on mars by sublimation of unstable equatorial ice during low obliquity. *Nature* 431, 1072–1075.
- Levy, J., Head, J.W., Marchant, D.R., 2010. Concentric crater fill in the northern mid-latitudes of Mars: formation processes and relationships to similar landforms of glacial origin. *Icarus* 209, 390–404.
- Li, L., Yue, Z., Di, K., Peng, M., 2015. Observations of martian layered ejecta craters and constraints on their formation mechanisms. *Meteorit. Planet. Sci.* 50, 508–522.
- Madeleine, J.B., Forget, F., Head, J.W., Levrard, B., Montmessin, F., Millour, E., 2009. Amazonian northern mid-latitude glaciation on Mars: a proposed climate scenario. *Icarus* 203, 390–405.
- Malin, M.C., Dzurisin, D., Sharp, R.P., 1983. Stripping of keanakoi tephra on kilaeua volcano, hawaii. *Geol. Soc. Am. Bull.* 94, 1148–1158.
- Marzo, G.A., Davila, A.F., Tornabene, L.L., Dohm, J.M., Fairen, A.G., Gross, C., et al., 2010. Evidence for hesperian impact-induced hydrothermalism on mars. *Icarus* 208, 667–683.
- Mellon, M.T., Jakosky, B.M., 1995. The distribution and behavior of martian ground ice during past and present epochs. *J. Geophys. Res.* 100, 11781–11799.
- Mellon, M.T., Arvidson, R.E., Sizemore, H.G., Searls, M.L., Blaney, D.L., Cull, S., et al., 2009. Ground ice at the phoenix landing site: stability state and origin. *J. Geophys. Res.* 114, E00E07.
- Melosh, H.J., 1989. *Impact Cratering: A Geologic Process*. Oxford University Press, New York.

- Middleton, G.V., 1970. Experimental studies related to problems of flysch sedimentation. In: Lajoie, J. (Ed.), *Flysch Sedimentology in North America*, pp. 253–272. edited by.
- Mouginis-Mark, P., 1979. Martian fluidized crater morphology: variations with crater size, latitude, altitude, and target material. *J. Geophys. Res.* 84, 8011–8022.
- Mouginis-Mark, P., 1981. Ejecta emplacement and modes of formation of martian fluidized ejecta craters. *Icarus* 45, 60–76.
- Mouginis-Mark, P.J., Hayashi, J.N., 1993. Shallow and deep fresh impact craters in hesperium planum, mars. *Earth Moon Planets* 61, 1–20.
- Mouginot, J., Pommerol, A., Kofman, W., Beck, P., Schmitt, B., Herique, A., et al., 2010. The 3–5 MHz global reflectivity map of mars by MARSIS/Mars Express: implications for the current inventory of subsurface H<sub>2</sub>O. *Icarus* 210, 612–625.
- Mouginot, J., Pommerol, A., Beck, P., Kofman, W., Clifford, S.M., 2012. Dielectric map of the martian northern hemisphere and the nature of plain filling materials. *Geophys. Res. Lett.* 39, L02202.
- Mustard, J.F., Cooper, C.D., Rifkin, M.K., 2001. Evidence for recent climate change on mars from the identification of youthful near-surface ground ice. *Nature* 412, 411–414.
- Nava, R.A., 2011. *Crater HelperTools for ArcGIS 10.0*. U.S. Geological Survey, Flagstaff, Ariz [ftp://pdsimage2.wr.usgs.gov/pub/pigpen/ArcMap\\_addons/](ftp://pdsimage2.wr.usgs.gov/pub/pigpen/ArcMap_addons/).
- Oberbeck, V.R., 1975. The role of ballistic erosion and sedimentation in lunar stratigraphy. *Rev. Geophys. Space Phys.* 13, 337–362.
- Oberbeck, V.R., 2009. Layered ejecta craters and the early water/ice aquifer on mars. *Meteorit. Planet. Sci.* 44, 43–54.
- Osinski, G.R., 2006. Effect of volatiles and target lithology on the generation and emplacement of impact crater fill and ejecta deposits on mars. *Meteorit. Planet. Sci.* 41, 1571–1586.
- Osinski, G.R., Spray, J.G., Lee, P., 2001. Impact-induced hydrothermal activity within the haughton impact structure, arctic Canada: generation of a transient, warm, wet oasis. *Meteor. Planet. Sci.* 36, 731–745.
- Osinski, G.R., Soare, R.J., 2007. Circular structures in utopiaplanitia, mars: impact v. periglacial origin and implications for assessing ground-ice content. 38th Lunar and Planetary Science Conference Abstract #1609.
- Osinski, G.R., Tornabene, L.L., Grieve, R.A., 2011. Impact ejecta emplacement on terrestrial planets. *Earth Planet. Sci. Lett.* 310, 167–181.
- Osinski, G.R., Tornabene, L.L., Baerjee, N.R., Cockell, C.S., Flemming, R., Izawa, M.R., et al., 2013. Impact-generated hydrothermal systems on earth and mars. *Icarus* 224, 347–363.
- Pike, R.J., 1980. Formation of complex impact craters: evidence from mars and other planets. *Icarus* 43, 1–19.
- Plaut, J.J., Safaeinili, A., Holt, J.W., Phillips, R.J., Head, J.W., Seu, R., et al., 2009. Radar evidence for ice in lobate debris aprons in the mid-northern latitudes of mars. *Geophys. Res. Lett.* 36, L02203.
- Robbins, S.J., Hynek, B.M., 2012. A new global database of mars impact craters >1km: 1. Database creation, properties, and parameters. *J. Geophys. Res.* 117, E05004.
- Schorghofer, N., Forget, F., 2012. History and anatomy of subsurface ice on mars. *Icarus* 220, 1112–1120.
- Schultz, P.H., 1992. Atmospheric effects on ejecta emplacement. *J. Geophys. Res.* 97, 11623–11662.
- Schultz, P.H., Gault, D.E., 1979. Atmospheric effects on martian ejecta emplacement. *J. Geophys. Res.* 84, 7669–7687.
- Senft, L.E., Stewart, S.T., 2008. Impact crater formation in icy layered terrains on mars. *Meteorit. Planet. Sci.* 43, 1993–2013.
- Sizemore, H.G., Zent, A.P., Rempel, A.W., 2015. Initiation and growth of martian ice lenses. *Icarus* 251, 191–210.
- Smith, P.H., Tamppari, L.K., Arvidson, R.E., Bass, D., Blaney, D., Boynton, W.V., et al., 2009. H<sub>2</sub>O at the phoenix landing site. *Science* 325, 58–61.
- Soare, R.J., Burr, D.M., Tseung, WanBun, M., J., 2005. Possible pingos and a periglacial landscape in utopiaplanitia. *Icarus* 174, 373–382.
- Stepinski, T.F., Mendenhall, M.P., Bue, B.D., 2009. Machine cataloging of impact craters on mars. *Icarus* 203, 77–87.
- Tanaka, K.L., Skinner, J.A., Dohm, J.M., Irwin, R.P., Kolb, E.J., Fortezzo, C.M., et al. (2014). *Geologic map of Mars: U.S. Geological Survey Scientific Investigations Map 3292, scale 1:20,000,000*.
- Viola, D., McEwen, A.S., Dundas, C.M., Byrne, S., 2015. Expanded secondary craters in the arcadiaplanitia region, Mars: evidence for tens of Myr-old shallow subsurface ice. *Icarus* 248, 190–204.
- Wada, K., Barnouin-Jha, S., 2006. The formation of fluidized ejecta on mars by granular flows. *Meteorit. Planet. Sci.* 41, 1551–1569.
- Weiss, D.K., Head, J.W., 2013. Formation of double-layered ejecta craters on Mars: a glacial substrate model. *Geophys. Res. Lett.* 40, 3819–3824.
- Weiss, D.K., Head, J.W., 2014. Ejecta mobility of layered ejecta craters on Mars: assessing the influence of snow and ice deposits. *Icarus* 233, 131–146.
- Wohletz, K.H., Sheridan, M.F., 1983. Martian rampart crater ejecta: experiments and analysis of melt-water interaction. *Icarus* 56, 15–37.
- Wulf, G., Kenkmann, T., 2015. High-resolution studies of double-layered ejecta craters: Morphology, inherent structure, and phenomenological formation model. *Meteorit. Planet. Sci.* 50, 173–203.
- Wulf, G., Pietrek, A., Kenkmann, T., 2013. Blocks and megablocks in the ejecta layers of a double-layer-ejecta (DLE) crater on mars. 44th Lunar and Planetary Science Conference Abstract #1453.
- Xiao, Z., Komatsu, G., 2013. Impact craters with ejecta flows and central pits on mercury. *Planet. Space Sci.* 82–83, 62–78.
- Zanetti, M., Hiesinger, H., Reiss, D., Hauber, E., Neukum, G., 2010. Distribution and evolution of scalloped terrain in the southern hemisphere, mars. *Icarus* 206, 691–706.
- Zimbelman, J.R., 1990. Outliers of dust along the southern margin of the tharsis Region, mars. In: *Proceedings of the 20th Lunar and Planetary Science Conference*. Houston, Tex, pp. 525–530.
- Zimbelman, J.R., Clifford, S.M., Williams, S.H., 1989. Concentric crater fill on Mars: an aeolian alternative to ice-rich mass wasting. In: *Proceedings of the 19th Lunar and Planetary Science Conference*. Houston, Tex, pp. 397–407.
- Zurcher, L., Kring, D.A., 2004. Hydrothermal alteration in the core of the Yaxcopoil-1 borehole, chichulub impact structure, Mexico. *Meteorit. Planet. Sci.* 39, 1199–1221.